

Concurrent Implicit Spectral Deferred Correction Scheme for Low-Mach Number Combustion with Detailed Chemistry

François P. Hamon^{a,*}, Marcus S. Day^a, Michael L. Minion^a

^aCenter for Computational Sciences and Engineering, Lawrence Berkeley National Laboratory, Berkeley, USA

Abstract

We present a parallel multi-implicit time integration scheme for the advection-diffusion-reaction systems arising from the equations governing low-Mach number combustion with complex chemistry. Our strategy employs parallelization across the method to accelerate the serial Multi-Implicit Spectral Deferred Correction (MISDC) scheme used to couple the advection, diffusion, and reaction processes. In our approach, the diffusion solves and the reaction solves are performed concurrently by different processors. Our analysis shows that the proposed parallel scheme is stable for stiff problems and that the sweeps converge to the fixed-point solution at a faster rate than with serial MISDC. We present numerical examples to demonstrate that the new algorithm is high-order accurate in time, and achieves a parallel speedup compared to serial MISDC.

Keywords: low-Mach number combustion, complex chemistry, time integration, multi-implicit spectral deferred corrections, parallelization across the method

1. Introduction

Many reacting flow problems are modeled by advection-diffusion-reaction partial differential equations. These systems are often characterized by a large disparity in the time scales of these three processes, therefore making the design of accurate and efficient time integration schemes particularly challenging. This is the case for the low-Mach number combustion approaches used to simulate laboratory-scale flames. Low-Mach number combustion models are obtained from the fully compressible equations by an asymptotic analysis which eliminates the fast acoustic waves while still accounting for compressibility effects caused by diffusion and reaction processes (Majda and Sethian, 1985). This methodology is advantageous for the computational efficiency of the time integration scheme because low-Mach number combustion models can therefore be numerically evolved on the time scale of the relatively slow advection process. The resulting stability constraint is much less restrictive than in fully compressible models and significantly larger stable time steps can be used. However, this approach requires a sophisticated integration method to couple advection with the diffusion and reaction processes which operate on much faster time scales. The coupling strategy becomes a key determinant of the largest time step size that preserves the accuracy, stability, and computational efficiency of the overall numerical simulation framework.

A popular approach to advance low-Mach number reactive systems is operator splitting, in which the different physical processes are decoupled and solved sequentially. Operator splitting is attractive because it allows specialized schemes and solvers to be used for advection, diffusion, and reaction, with different time step sizes depending on the stiffness of each process. Applications to low-Mach number combustion include the second-order Strang-split schemes of Knio et al. (1999); Day and Bell (2000). The former is based on an explicit evaluation of the advection and diffusion terms and an implicit treatment of the reaction term. The latter couples an explicit scheme for advection with a Crank-Nicolson treatment of diffusion and a fully implicit method for reactions; the implicit diffusion treatment accommodates that diffusive time scales in combustion can be much shorter than those of advective

*Corresponding author

transport. Several authors present alternatives to address the stiffness of the diffusion terms relative to advection via extended-stability Runge-Kutta-Chebyshev schemes (Najm and Knio, 2005; Safta et al., 2010; Motheau and Abraham, 2016). However, in all such attempts, the underlying splitting approach introduces significant time-splitting errors, and therefore requires a dynamic adaptation of the time step sizes to preserve the accuracy of the approximation, as in Duarte et al. (2013). In addition to this drawback, a significant limitation of operator-splitting approaches in general is that they cannot be easily extended beyond second-order accuracy in time.

Recently, the Multi-Implicit Spectral Deferred Correction (MISDC) scheme of Bourlioux et al. (2003); Layton and Minion (2004) has been successfully employed to couple advection, diffusion, and reaction processes in the low-Mach number equation set (Nonaka et al., 2012; Pazner et al., 2016). The methodology builds on the Semi-Implicit Spectral Deferred Correction (SISDC) scheme of Minion (2003) and aims at handling a right-hand side with one or more explicit terms coupled with multiple implicit terms. Specifically, MISDC relies on a temporal splitting in which advection is treated explicitly while diffusion and reaction are treated implicitly but decoupled as in operator splitting. In MISDC, the integration is based on a sequence of low-order corrections applied to the variables to iteratively achieve high-order accuracy. At a given Spectral Deferred Correction (SDC) temporal node, the diffusion and reaction corrections are computed separately in two successive implicit solves. Numerical results showed that MISDC is able to accurately resolve stiff kinetics while capturing the coupling between chemical reactions and transport processes. The finite-volume schemes based on MISDC avoid the often catastrophic splitting errors of Strang splitting, while also reducing the cost of the implicit reaction solves and achieving second-order space-time accuracy in Nonaka et al. (2012), and fourth-order in Pazner et al. (2016).

The implicit solves corresponding to the diffusion and reaction steps still represent most of the computational cost incurred by the multi-implicit time integration scheme for these stiff advection–diffusion–reaction systems. In the numerical methodology for low-Mach number combustion presented in Pazner et al. (2016), the treatment of the diffusion and reaction steps is sequential to avoid solving a global diffusion-reaction nonlinear system involving all the degrees of freedom. Instead, the diffusion step requires solving a linearized system for each mass conservation equation and for the energy equation to update the species mass fractions and the enthalpy. Then, the diffusion step is followed by the reaction step to update the species mass fractions. The latter entails solving complex, but local, nonlinear Newton-based backward-Euler systems to evolve the multistep kinetic network of the combustion process under consideration. These sequential solves become very expensive for detailed combustion problems with a large number of species involved in stiff and highly nonlinear chemical reaction paths.

In this paper, we design a multi-implicit spectral deferred correction-based integration method in which the implicit diffusion and reaction steps are performed concurrently to overcome the sequential limitation of the standard MISDC method. Our algorithm, referred to as Concurrent Implicit SDC (CISDC), relies on *parallelization across the method* according to the classification of Burrage (1997). Examples of parallel-across-the-method approaches include Runge-Kutta schemes in which intermediate stage values are computed in parallel (Iserles and Nørsett, 1990; Butcher, 1997), and SDC schemes in which the corrections are applied at multiple temporal nodes concurrently (Christlieb et al., 2010; ?). This strategy can be contrasted with *parallelization across the steps* (Nievergelt, 1964; Miranker and Liniger, 1967; Lions et al., 2001; Emmett and Minion, 2012; Falgout et al., 2014) in which the parallel work is done on multiple time steps concurrently, and *parallelization across the problem* (e.g. waveform relaxation methods (Lelarasmee et al., 1982; Gander, 1999)), in which the problem is divided into temporal subproblems solved simultaneously.

In the proposed CISDC algorithm, we formally decouple the diffusion step at a given SDC temporal node from the reaction step at the previous node. These two steps are therefore independent and can be executed in parallel by multiple processors. In this work, we focus primarily on the convergence of the correction iterations to show that the parallel scheme retains robust stability properties for stiff problems, which is key for combustion problems with complex chemistry. We also analyze the theoretical computational cost of the proposed CISDC scheme. Then, we modify the numerical methodology of Pazner et al. (2016) to perform the temporal integration of the low-Mach number equation set with our parallel-across-the-method scheme. Finally, we demonstrate the robustness and efficiency of the new approach using synthetic test cases and a challenging one-dimensional unsteady flame simulation.

We proceed to the presentation of the low-Mach number equation set in Section 2. In Section 3, we

propose our parallel Concurrent Implicit SDC scheme in which the implicit solves can be performed in parallel to reduce the computational cost. The stability and convergence properties of the scheme are analyzed in Section 4. Numerical examples are presented in Section 5.

2. Low-Mach number governing equations

Following previous work by Day and Bell (2000); Nonaka et al. (2012); Pazner et al. (2016), we consider a low-Mach number model presented by Rehm and Baum (1978) and derived from an asymptotic analysis in Majda and Sethian (1985). It consists of a system of partial differential equations governing the evolution of a gaseous mixture in an open container in a non-gravitationally stratified environment. The system describes coupled advection, differential/preferential diffusion, and chemical reaction processes, and relies on a mixture model for species diffusion (Kee et al., 1983; Warnatz and Peters, 1982). The Soret and Dufour transport effects are ignored. Sound waves are analytically eliminated from the system, but the local compressibility effects caused by reactions and diffusion are included in the model. The system is closed by an equation of state (EOS), written as a constraint on the divergence of the velocity, which acts to ensure that the thermodynamic pressure remains constant over space and time. Physically, this approach amounts to enforcing an instantaneous acoustic equilibration of the entire system to the constant ambient pressure.

Considering a mixture with N species, conservation of mass for species $i \in \{1, \dots, N\}$, and conservation of energy are expressed by the evolution equations

$$\frac{\partial(\rho Y_i)}{\partial t} = -\nabla \cdot (U \rho Y_i) + \nabla \cdot \rho \mathcal{D}_i \nabla Y_i + \dot{\omega}_i, \quad i \in \{1, \dots, N\}, \quad (1)$$

$$\frac{\partial(\rho h)}{\partial t} = -\nabla \cdot (U \rho h) + \nabla \cdot \frac{\lambda}{c_p} \nabla h + \sum_i \nabla \cdot h_i \left(\rho \mathcal{D}_i - \frac{\lambda}{c_p} \right) \nabla Y_i, \quad (2)$$

where ρ is the density, $\mathbf{Y} = [Y_1, \dots, Y_N]$ are the species mass fractions, $\mathcal{D}_i(\mathbf{Y}, T)$ is the mixture-averaged diffusion coefficient of species i , T is the temperature, $\dot{\omega}_i(\mathbf{Y}, T)$ is the production rate of species i due to chemical reactions, $h(\mathbf{Y}, T) = \sum_i Y_i h_i(T)$ is the enthalpy with $h_i(T)$ denoting the enthalpy of species i , $\lambda(\mathbf{Y}, T)$ is the thermal conductivity, and $c_p = \sum_i Y_i dh_i/dT$ is the specific heat at constant pressure. In this formulation, there is no exchange in enthalpy due to chemical reactions since h includes the standard enthalpy of formation. These evolution equations are closed by an EOS, which states that the thermodynamic pressure, p_{EOS} , must remain constant and equal to the ambient pressure, p_0 ,

$$p_0 = p_{EOS}, \quad (3)$$

where p_{EOS} is computed as

$$p_{EOS} := \rho \mathcal{R} T \sum_i \frac{Y_i}{W_i}. \quad (4)$$

\mathcal{R} is the universal gas constant and W_i is the molecular weight of species i . In the mixture model considered here, the diffusion flux, Γ_i , of species i , is defined as $\Gamma_i := -\rho \mathcal{D}_i \nabla Y_i$. To enforce that the sum of the fluxes is equal to zero and therefore to guarantee mass conservation, we define a dominant species, i_0 , whose diffusion flux is set to $\Gamma_{i_0} := -\sum_{i \neq i_0} \Gamma_i$. Using this approach, one can sum the species equation (1) to obtain the continuity equation,

$$\frac{\partial \rho}{\partial t} = -\nabla \cdot (U \rho), \quad (5)$$

where we used the constraints

$$\sum_i Y_i = 1, \quad \text{and} \quad \sum_i \dot{\omega}_i = 0. \quad (6)$$

A possible approach consists in evolving all the thermodynamic variables but one with (1)-(2), and then use the EOS (3) to compute the last thermodynamic variable (Najm et al., 1998; Knio et al., 1999). However, this approach fails to strictly conserve energy. Instead, we follow the volume discrepancy method

of Pember et al. (1998); Day and Bell (2000). That is, the EOS (3) is written in the form of a constraint on the divergence of the velocity. This is achieved by taking the derivative of (3) in the Lagrangian frame while enforcing that the thermodynamic pressure remains constant, and then substituting the evolution equations (1)-(2) for ρ , \mathbf{Y} , and T to obtain

$$\nabla \cdot \mathbf{U} = S. \quad (7)$$

The quantity S is defined as

$$S := \frac{1}{\rho c_p T} \left(\nabla \cdot \lambda \nabla T + \sum_i \Gamma_i \cdot \nabla h_i \right) + \frac{1}{\rho} \sum_i \frac{W}{W_i} \nabla \cdot \Gamma_i + \frac{1}{\rho} \sum_i \left(\frac{W}{W_i} - \frac{h_i}{c_p T} \right) \dot{\omega}_i, \quad (8)$$

where $W = (\sum_i Y_i/W_i)^{-1}$ denotes the mixture-averaged molecular weight. Equations (7)-(8) represent a linearized approximation to the velocity field required to hold the thermodynamic pressure equal to p_0 in the presence of local compressibility effects due to reaction heating, compositional changes, and thermal diffusion. In summary, the system of partial differential equations solved in this work is given by (1), (2), and (5), coupled with the velocity constraint, (7)-(8). As an aside, since we only consider the one-dimensional case in the present work, the numerical scheme does not require a velocity projection; the velocity is fully determined via the divergence constraint (7) and the inflow Dirichlet boundary condition specified in the numerical examples. Next, we proceed to the description of the temporal discretization applied to these PDEs, with an emphasis on the proposed parallel spectral deferred correction scheme.

3. Parallel spectral deferred correction scheme

3.1. Multi-implicit spectral deferred correction schemes

We start with a review of the fundamentals of the Spectral Deferred Correction (SDC) and Multi-Implicit Spectral Deferred Correction (MISDC) schemes. Consider the ODE on a generic time step

$$\phi_t(t) = F_A(\phi(t)) + F_D(\phi(t)) + F_R(\phi(t)), \quad t \in [t^n, t^n + \Delta t], \quad (9)$$

$$\phi(t^n) = \phi^n, \quad (10)$$

and its solution in integral form given by

$$\phi(t) = \phi^n + \int_{t^n}^t F(\phi(\tau)) d\tau, \quad (11)$$

where F_A , F_D , and F_R represent the advection, diffusion, and reaction terms, respectively, with $F = F_A + F_D + F_R$. We denote by $\tilde{\phi}(t)$ the approximation of $\phi(t)$, and we define the correction $\delta(t) := \phi(t) - \tilde{\phi}(t)$. The SDC scheme of Dutt et al. (2000) iteratively improves the accuracy of the approximation with the update equation

$$\begin{aligned} \tilde{\phi}(t) + \delta(t) &= \phi^n + \int_{t^n}^t [F(\tilde{\phi}(\tau) + \delta(\tau)) - F(\tilde{\phi}(\tau))] d\tau \\ &\quad + \int_{t^n}^t F(\tilde{\phi}(\tau)) d\tau. \end{aligned} \quad (12)$$

In (12), the first integral is approximated with a low-order discretization such as backward- or forward-Euler, whereas the second integral is approximated with a high-order quadrature rule. The resulting discrete update is applied iteratively in sweeps to increase the order of accuracy of the approximation. Specifically, each sweep increases the formal order of accuracy by one until the order of accuracy of the quadrature applied to the second integral is reached (Hagstrom and Zhou, 2007; Xia et al., 2007; Christlieb et al., 2009).

MISDC, proposed in Bourlioux et al. (2003); Layton and Minion (2004), and used in Pazner et al. (2016), is based on a variant of the original SDC update equation (12). It is well suited for advection-diffusion-reaction problems in which the time scales corresponding to these three processes are very

different, which is the case for low-Mach number combustion with complex chemistry. MISDC provides a methodology to treat these processes sequentially while accounting for the physical coupling between them to minimize the splitting error. This approach is based on the update equations

$$\begin{aligned}\tilde{\phi}(t) + \delta_A(t) &= \phi^n + \int_{t^n}^t [F_A(\tilde{\phi}(\tau) + \delta_A(\tau)) - F_A(\tilde{\phi}(\tau))] d\tau \\ &\quad + \int_{t^n}^t F(\tilde{\phi}(\tau)) d\tau,\end{aligned}\tag{13}$$

$$\begin{aligned}\tilde{\phi}(t) + \delta_{AD}(t) &= \phi^n + \int_{t^n}^t [F_A(\tilde{\phi}(\tau) + \delta_A(\tau)) - F_A(\tilde{\phi}(\tau)) + F_D(\tilde{\phi}(\tau) + \delta_{AD}(\tau)) - F_D(\tilde{\phi}(\tau))] d\tau \\ &\quad + \int_{t^n}^t F(\tilde{\phi}(\tau)) d\tau,\end{aligned}\tag{14}$$

$$\begin{aligned}\tilde{\phi}(t) + \delta(t) &= \phi^n + \int_{t^n}^t [F_A(\tilde{\phi}(\tau) + \delta_A(\tau)) - F_A(\tilde{\phi}(\tau)) + F_D(\tilde{\phi}(\tau) + \delta_{AD}(\tau)) - F_D(\tilde{\phi}(\tau)) \\ &\quad + F_R(\tilde{\phi}(\tau) + \delta(\tau)) - F_R(\tilde{\phi}(\tau))] d\tau + \int_{t^n}^t F(\tilde{\phi}(\tau)) d\tau.\end{aligned}\tag{15}$$

To discretize the update equations, SDC-based methods rely on a decomposition of the time interval $[t^n, t^{n+1}]$ into M subintervals using $M + 1$ temporal nodes, such that

$$t^n = t^{n,0} < t^{n,1} < \dots < t^{n,M} = t^n + \Delta t = t^{n+1}.\tag{16}$$

In this work, we consider Gauss-Lobatto nodes for the definition of the subintervals. For brevity, we use the shorthand notations $t^m = t^{n,m}$ and $\Delta t^m = t^{m+1} - t^m$ in the remainder of the paper. We denote by $\phi^{m,(k)}$ the approximation of $\phi(t^m)$ at sweep (k) . In the application considered here, the diffusion and reaction terms are very stiff compared to the advection term which operates on a much slower time scale. Therefore, in MISDC the diffusion and reaction terms are treated implicitly and discretized with a backward-Euler method, whereas the advection term is treated explicitly and discretized with a forward-Euler method. Based on this temporal splitting, computing $\phi_A^{m+1,(k+1)}$ is not necessary, and the updates (13)-(14)-(15) simplify to the discrete update equations

$$\begin{aligned}\phi_{AD}^{m+1,(k+1)} &= \phi^{m,(k+1)} + \Delta t^m [F_A(\phi^{m,(k+1)}) - F_A(\phi^{m,(k)}) \\ &\quad + F_D(\phi_{AD}^{m+1,(k+1)}) - F_D(\phi^{m+1,(k)})] + \Delta t S^{m:m+1}(F(\phi^{(k)})),\end{aligned}\tag{17}$$

$$\begin{aligned}\phi^{m+1,(k+1)} &= \phi^{m,(k+1)} + \Delta t^m [F_A(\phi^{m,(k+1)}) - F_A(\phi^{m,(k)}) \\ &\quad + F_D(\phi_{AD}^{m+1,(k+1)}) - F_D(\phi^{m+1,(k)})] \\ &\quad + F_R(\phi^{m+1,(k+1)}) - F_R(\phi^{m+1,(k)}) + \Delta t S^{m:m+1}(F(\phi^{(k)})),\end{aligned}\tag{18}$$

where $S^{m:m+1}(F(\phi^{(k)}))$ is a high-order numerical quadrature approximating the last integral in (12) over the interval between two consecutive SDC nodes using the Lagrange polynomials L_j , $j \in \{0, \dots, M\}$,

$$S^{m:m+1}(F(\phi^{(k)})) := \sum_{j=0}^M s_{m+1,j} F(\phi^{(k)}),\tag{19}$$

with

$$s_{m+1,j} := \frac{1}{\Delta t} \int_{t^m}^{t^{m+1}} L_j(\tau) d\tau.\tag{20}$$

Weiser (2015) proposed a new class of SDC schemes in which the SDC sweep is cast as a stage of a diagonally implicit Runge-Kutta method. The choice of quadrature weights, based on LU decomposition,

leads to a faster convergence of the iterative correction process than simpler backward-Euler. This new approach is also advantageous because in the resulting scheme, the sweeps remain convergent when the underlying problem is very stiff. Here, we adapt the scheme of Weiser (2015) to our multi-implicit framework based on Gauss-Lobatto nodes by writing the update equations for $m \in \{0, \dots, M-1\}$ as

$$\begin{aligned} \phi_{AD}^{m+1,(k+1)} &= \phi^0 + \Delta t \sum_{j=1}^m \tilde{q}_{m+1,j}^E [F_A(\phi^{j,(k+1)}) - F_A(\phi^{j,(k)})] \\ &\quad + \Delta t \sum_{j=1}^m \tilde{q}_{m+1,j}^I [F_D(\phi^{j,(k+1)}) - F_D(\phi^{j,(k)})] \\ &\quad + \Delta t \tilde{q}_{m+1,m+1}^I [F_D(\phi_{AD}^{m+1,(k+1)}) - F_D(\phi^{m+1,(k)})] \\ &\quad + \Delta t Q^{0:m+1}(F(\phi^{(k)})), \end{aligned} \tag{21}$$

$$\begin{aligned} \phi^{m+1,(k+1)} &= \phi^0 + \Delta t \sum_{j=1}^m \tilde{q}_{m+1,j}^E [F_A(\phi^{j,(k+1)}) - F_A(\phi^{j,(k)})] \\ &\quad + \Delta t \sum_{j=1}^m \tilde{q}_{m+1,j}^I [F_D(\phi^{j,(k+1)}) - F_D(\phi^{j,(k)}) + F_R(\phi^{j,(k+1)}) - F_R(\phi^{j,(k)})] \\ &\quad + \Delta t \tilde{q}_{m+1,m+1}^I [F_D(\phi_{AD}^{m+1,(k+1)}) - F_D(\phi^{m+1,(k)}) + F_R(\phi^{m+1,(k+1)}) - F_R(\phi^{m+1,(k)})] \\ &\quad + \Delta t Q^{0:m+1}(F(\phi^{(k)})), \end{aligned} \tag{22}$$

where $Q^{0:m+1}(F(\phi^{(k)}))$ approximates the integral of F over the temporal interval $[t^0, t^{m+1}]$,

$$Q^{0:m+1}(F(\phi^{(k)})) := \sum_{j=0}^M q_{m+1,j} F(\phi^{(k)}), \tag{23}$$

with

$$q_{m+1,j} := \frac{1}{\Delta t} \int_{t^0}^{t^{m+1}} L_j(\tau) d\tau. \tag{24}$$

We denote by $\mathbf{Q} = \{q_{i,j}\} \in \mathbb{R}^{M \times (M+1)}$ the matrix containing the weights defined in (24). We decompose \mathbf{Q} into its first column $\mathbf{q} \in \mathbb{R}^M$, and the matrix containing the remaining M columns, denoted by $\tilde{\mathbf{Q}} \in \mathbb{R}^{M \times M}$. The coefficients $\{\tilde{q}_{i,j}^I\}$ in $\tilde{\mathbf{Q}}^I \in \mathbb{R}^{M \times M}$ are obtained by setting

$$\tilde{\mathbf{Q}}^I := \tilde{\mathbf{U}}^T, \tag{25}$$

where $\tilde{\mathbf{U}}^T$ is the transpose of the upper triangular matrix in the LU decomposition of $\tilde{\mathbf{Q}}^T$. We refer to Weiser (2015) for a detailed discussion of the implications of this choice of coefficients on the convergence of the SDC iterations in the case of Gauss-Radau nodes. Finally, the coefficients $\{\tilde{q}_{i,j}^E\}$ in $\tilde{\mathbf{Q}}^E \in \mathbb{R}^{M \times M}$ are set to $\tilde{q}_{m+1,m}^E := \Delta t^m / \Delta t$, and $\tilde{q}_{m+1,j \neq m+1}^E := 0$, corresponding to forward-Euler.

In the remainder of this paper, the modified MISDC scheme of (21)-(22) will be referred to as MISDCQ. In the convergence analysis of Section 4 and in numerical examples of Section 5, we will show that for stiff problems, MISDCQ converges to the fixed-point solution in fewer sweeps than the standard MISDC of (17)-(18). Next, we use MISDCQ as a basis for the construction of a parallel-across-the-method Concurrent Implicit SDC scheme.

3.2. Concurrent implicit spectral deferred correction scheme

In the MISDC and MISDCQ schemes, the implicit solves corresponding to the diffusion and reaction steps represent most of the computational cost of the temporal integration scheme. At each SDC node, these solves are performed sequentially, with the reaction step following the diffusion step. These solves can become expensive for highly resolved combustion problems with a large number of species involved in a stiff and highly nonlinear chemical reaction path. In this section, we design a stable parallel-across-the-method Concurrent Implicit Spectral Deferred Correction (CISDC) scheme in which the implicit diffusion and reaction solves can be performed concurrently.

3.2.1. Decoupling strategy

In the MISDCQ scheme (21)-(22), the diffusion step at node $m + 1$ depends on the output of the reaction step at node m , denoted by $\phi^{m,(k+1)}$. Then, the output of the diffusion step at node $m + 1$, denoted by $\phi_{AD}^{m+1,(k+1)}$, is used to compute the reaction step at node $m + 1$, and obtain $\phi^{m+1,(k+1)}$. The MISDCQ algorithm is therefore inherently serial across the sweeps and cannot be parallelized without modification. We overcome this limitation by formally decoupling the diffusion and reaction steps to compute them concurrently.

There are multiple ways to achieve this goal. A simple strategy to decouple the diffusion and reaction steps consists in lagging the index (k) in (21), i.e., to use a lagged diffusion term, $\phi_{AD}^{m+1,(k)}$, in the computation of the reaction term, $\phi^{m+1,(k+1)}$. This decoupling allows a concurrent update of the diffusion and reaction terms at the same node, $m + 1$. With this approach, M steps are needed to update the state variables at the M SDC nodes. But, we found that his approach led to unstable schemes for stiff problems and therefore we do not further discuss it here.

Instead, we adopt a decoupling strategy that allows a concurrent update of the diffusion and reaction terms at two consecutive SDC nodes. Specifically, in the proposed marching scheme, we solve in parallel the diffusion step at node $m + 1$ and the reaction step at the previous node, m . A sketch of this parallel marching scheme is in Fig. 1. We highlight that this algorithm requires $M + 1$ steps to traverse the M SDC nodes – that is, one additional step compared to the approach outlined in the previous paragraph –, but remains stable for the stiff problems considered in this work, as shown in Section 4.

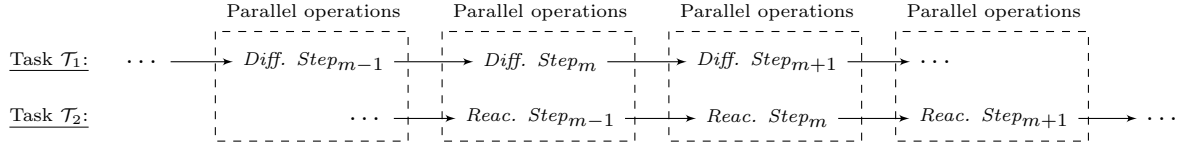


Figure 1: Sketch of the sweep parallelization strategy based on a decoupling of the diffusion step at $m + 1$ from the reaction step at m to solve them concurrently.

The parallel marching scheme described in Fig. 1 is achieved by lagging in SDC sweep the terms that introduce a dependence on the reaction step at node m in the diffusion step at node $m + 1$. Specifically, in the diffusion solve at node $m + 1$ of sweep ($k + 1$), we replace $F_A(\phi^{m,(k+1)})$, $F_D(\phi^{m,(k+1)})$, and $F_R(\phi^{m,(k+1)})$ with lagged values $F_A(\phi^{m,(k+1,0)})$, $F_D(\phi^{m,(k+1,0)})$, and $F_R(\phi^{m,(k+1,0)})$. Using these lagged values, the temporal interval is traversed to compute the corrected values $\phi_{AD}^{m+1,(k+1,1)}$ and $\phi^{m,(k+1,1)}$ in parallel at all SDC nodes using the parallelization strategy sketched in Fig. 1. The accuracy of the approximation is improved iteratively by repeating this procedure, i.e., at iteration $\ell + 1$, we correct $\phi_{AD}^{m+1,(k+1,\ell+1)}$ and $\phi^{m,(k+1,\ell+1)}$ in parallel at all nodes using lagged values computed at iteration ℓ . This results in a loop on ℓ nested in sweep ($k + 1$). At node $m + 1 \in \{1, \dots, M + 1\}$, each correction entails solving the update equations

$$\begin{aligned}
 \phi_{AD}^{m+1,(k+1,\ell+1)} &= \phi^0 + \Delta t \sum_{j=1}^{m-1} \tilde{q}_{m+1,j}^E [F_A(\phi^{j,(k+1,\ell+1)}) - F_A(\phi^{j,(k)})] \\
 &+ \Delta t \sum_{j=1}^{m-1} \tilde{q}_{m+1,j}^I [F_D(\phi^{j,(k+1,\ell+1)}) - F_D(\phi^{j,(k)}) + F_R(\phi^{j,(k+1,\ell+1)}) - F_R(\phi^{j,(k)})] \\
 &+ \Delta t \tilde{q}_{m+1,m}^E [F_A(\phi^{m,(k+1,\ell)}) - F_A(\phi^{m,(k)})] \\
 &+ \Delta t \tilde{q}_{m+1,m}^I [F_D(\phi^{m,(k+1,\ell)}) - F_D(\phi^{m,(k)}) + F_R(\phi^{m,(k+1,\ell)}) - F_R(\phi^{m,(k)})] \\
 &+ \Delta t \tilde{q}_{m+1,m+1}^I [F_D(\phi_{AD}^{m+1,(k+1,\ell+1)}) - F_D(\phi^{m+1,(k)}) + F_R(\phi^{m+1,(k+1,\ell)}) - F_R(\phi^{m+1,(k)})] \\
 &+ \Delta t Q^{0:m+1}(F(\phi^{(k)})), \tag{26}
 \end{aligned}$$

$$\begin{aligned}
\phi^{m+1,(k+1,\ell+1)} &= \phi^0 + \Delta t \sum_{j=1}^{m-1} \tilde{q}_{m+1,j}^E [F_A(\phi^{j,(k+1,\ell+1)}) - F_A(\phi^{j,(k)})] \\
&+ \Delta t \sum_{j=1}^{m-1} \tilde{q}_{m+1,j}^I [F_D(\phi^{j,(k+1,\ell+1)}) - F_D(\phi^{j,(k)}) + F_R(\phi^{j,(k+1,\ell+1)}) - F_R(\phi^{j,(k)})] \\
&+ \Delta t \tilde{q}_{m+1,m}^E [F_A(\phi^{m,(k+1,\ell)}) - F_A(\phi^{m,(k)})] \\
&+ \Delta t \tilde{q}_{m+1,m}^I [F_D(\phi^{m,(k+1,\ell)}) - F_D(\phi^{m,(k)}) + F_R(\phi^{m,(k+1,\ell+1)}) - F_R(\phi^{m,(k)})] \\
&+ \Delta t \tilde{q}_{m+1,m+1}^I [F_D(\phi_{AD}^{m+1,(k+1,\ell+1)}) - F_D(\phi^{m+1,(k)}) + F_R(\phi^{m+1,(k+1,\ell+1)}) - F_R(\phi^{m+1,(k)})] \\
&+ \Delta t Q^{0:m+1}(F(\phi^{(k)})), \tag{27}
\end{aligned}$$

where the matrices $\tilde{Q} = \{q_{ij}\}$, $\tilde{Q}^I = \{\tilde{q}_{ij}^I\}$, and $\tilde{Q}^E = \{\tilde{q}_{ij}^E\}$, are the same as in the MISDCQ method of Section 3.1. In (26) (respectively, (27)), the lagged terms – i.e., the terms evaluated at the previous iteration $\ell -$, are in the third, fourth, and fifth lines (respectively, third and fourth lines). A procedure is required to initialize these lagged terms at the first iteration. The lagged advection and diffusion terms are initialized using the most recent advection-diffusion update, whereas the lagged reaction term is initialized using the solution at the previous sweep, that is,

$$F_A(\phi^{m,(k+1,0)}) := F_A(\phi_{AD}^{m,(k+1,0)}), \tag{28}$$

$$F_D(\phi^{m,(k+1,0)}) := F_D(\phi_{AD}^{m,(k+1,0)}), \tag{29}$$

$$F_R(\phi^{j,(k+1,0)}) := F_R(\phi^{j,(k)}) \quad j \in \{m, m+1\}. \tag{30}$$

In the remainder of this paper, the scheme defined by (26) to (30) will be referred to as the Concurrent Implicit SDCQ (CISDCQ) scheme, since the implicit diffusion and reaction steps can be performed in parallel.

We highlight that unlike in MISDCQ, the CISDCQ diffusion step (26) at node $m+1$ contains a reaction correction. This correction is based on known values computed at the same iteration $\phi^{j,(k+1,\ell+1)}$ ($j \in \{1, \dots, m-1\}$) in the second line of (26), and on lagged values $\phi^{j,(k+1,\ell)}$ ($j \in \{m, m+1\}$) in the fourth and fifth lines of (26). Therefore, if the nested iteration on ℓ converges, computing $\phi^{m+1,(k+1,\ell+1)}$ in (26) yields an approximation of the solution obtained from an implicit fully coupled diffusion-reaction solve. The reaction step can then be seen as a correction of the error incurred by the lagged terms in the diffusion step. This becomes apparent when (26) is used to write (27) in the equivalent form

$$\begin{aligned}
\phi^{m+1,(k+1,\ell+1)} &= \phi_{AD}^{m+1,(k+1,\ell+1)} \\
&+ \Delta t \tilde{q}_{m+1,m}^I [F_R(\phi^{m,(k+1,\ell+1)}) - F_R(\phi^{m,(k+1,\ell)})] \\
&+ \Delta t \tilde{q}_{m+1,m+1}^I [F_R(\phi^{m+1,(k+1,\ell+1)}) - F_R(\phi^{m+1,(k+1,\ell)})]. \tag{31}
\end{aligned}$$

Using a linear convergence analysis in Section 4, we will demonstrate that this modification of the MISDCQ algorithm yields a stable integration scheme whose sweeps can converge to the fixed-point solution faster than the original MISDCQ.

3.2.2. Pipelining

The nested iteration scheme on ℓ used to improve the accuracy of the lagged terms in (26)-(27) increases the computational cost of a sweep since multiple iterations may be used at each sweep. However, this nested loop on ℓ can be performed efficiently, in parallel, when multiple iterations on ℓ are employed. This additional degree of parallelism, similar to the technique proposed in Christlieb et al. (2010, 2012), exploits the structure of the update equations (26)-(27).

We assume that at least two nested iterations on ℓ are used. As in Fig. 1, task \mathcal{T}_1 , which corresponds to the diffusion steps necessary to compute $\phi_{AD}^{m,(k+1,1)}$ ($m \in \{1, \dots, M\}$), and task \mathcal{T}_2 , which corresponds to the reaction steps needed to compute $\phi^{m,(k+1,1)}$ ($m \in \{1, \dots, M\}$), can be executed in parallel. But, as soon as $\phi^{1,(k+1,1)}$ has been computed, task \mathcal{T}_3 can be launched to perform the diffusion steps at the

next iteration ($\ell = 2$) and obtain $\phi_{AD}^{m,(k+1,2)}$ ($m \in \{1, \dots, M\}$) using the lagged values updated by task \mathcal{T}_2 . Then, once $\phi_{AD}^{1,(k+1,2)}$ is available, task \mathcal{T}_4 can be executed in parallel to compute the reaction updates $\phi^{m,(k+1,2)}$. This approach can be generalized to the case of 2ν tasks with $\nu \geq 2$. A sketch of this pipelined nested loop on ℓ is in Fig. 2.

The parallelism inherent in pipelining the substeps is assumed to be in addition to any spatial parallelization. Hence the term *processor* used here denotes a group of cores performing the parallel tasks in the CISDCQ algorithm. The number of tasks does not necessarily correspond to the number of processors used for the implementation of the algorithm as a given processor can be reused for multiple tasks. If three Gauss-Lobatto nodes are used ($M = 2$), only two diffusion steps and two reaction steps have to be performed at each nested iteration on ℓ . This means that when task \mathcal{T}_3 is launched, the two diffusion steps involved in task \mathcal{T}_1 have already been performed by the first processor which is now idling. Therefore, the first processor can be reused to perform task \mathcal{T}_3 . For the same reason, the second processor is idling after completing task \mathcal{T}_2 and can be reused to perform task \mathcal{T}_4 . With this strategy, the first processor performs tasks $\mathcal{T}_1, \mathcal{T}_3, \dots, \mathcal{T}_{2(\nu-1)-1}$ while the second processor performs tasks $\mathcal{T}_2, \mathcal{T}_4, \dots, \mathcal{T}_{2(\nu-1)}$. Similarly, if five Gauss-Lobatto nodes are used ($M = 4$), then at most four processors can be used. In the general case, the 2ν pipelined tasks involved in CISDCQ- ν use up to $\max(2\nu, M)$ processors working in parallel.

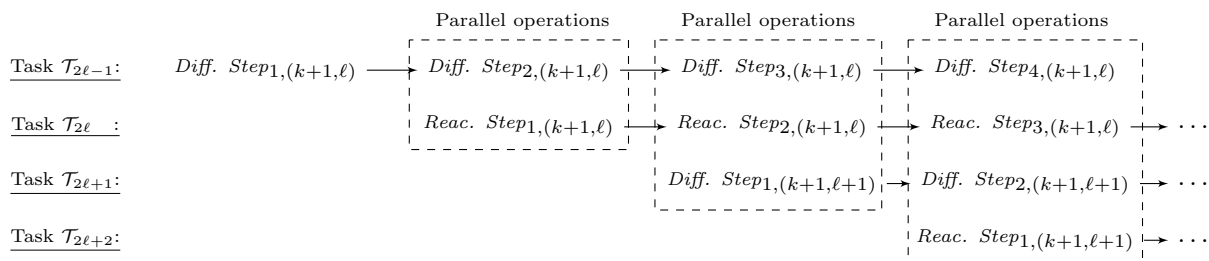


Figure 2: Sketch of the pipelined CISDCQ sweep with 2ν tasks for five Gauss-Lobatto nodes. The diffusion step $m + 1, (k + 1, \ell + 1)$ entails solving (26) for $\phi_{AD}^{m+1,(k+1,\ell+1)}$, and the reaction step $m + 1, (k + 1, \ell + 1)$ requires solving (27) for $\phi^{m+1,(k+1,\ell+1)}$.

To assess the computational cost reduction generated by the CISDCQ algorithm, we assume that the cost of a diffusion step (respectively, a reaction step) is a constant Υ_{AD} (respectively, Υ_R). N_M (respectively, N_C) denotes the number of sweeps required to achieve convergence with MISDCQ (respectively, CISDCQ). For a time interval $[t^n, t^{n+1}]$ decomposed into M subintervals using $M + 1$ temporal nodes, the computational cost of MISDCQ, C_M , is given by

$$C_M = N_M M (\Upsilon_{AD} + \Upsilon_R). \quad (32)$$

In the evaluation of the computational cost of CISDCQ, C_C , we neglect the communication costs and assume that ν iterations on ℓ are nested in each sweep to improve the accuracy of the lagged terms. First, we compute the cost of iteration $\ell + 1$ in sweep $(k + 1)$, i.e., the cost of the operations performed in tasks $\mathcal{T}_{2\ell+1}$ and $\mathcal{T}_{2\ell+2}$ (see Fig. 2). These operations include the initial diffusion step to compute $\phi_{AD}^{1,(k+1,\ell+1)}$, followed by $(M - 1)$ parallel diffusion and reaction steps, and by the final reaction step to compute $\phi^{M,(k+1,\ell+1)}$. Therefore, the cost of an iteration on ℓ nested in sweep $(k + 1)$ is

$$\Upsilon_{AD} + (M - 1) \max(\Upsilon_{AD}, \Upsilon_R) + \Upsilon_R. \quad (33)$$

Task $\mathcal{T}_{2\ell+1}$ can only start after task $\mathcal{T}_{2\ell-1}$ has computed $\phi_{AD}^{2,(k+1,\ell)}$ and after task $\mathcal{T}_{2\ell}$ has used this updated value to calculate $\phi^{2,(k+1,\ell)}$. The total cost of these two operations is $\Upsilon_{AD} + \Upsilon_R$. Using this result along with (33), we find by induction on ℓ that the cost of the CISDCQ sweep with ν nested iterations on ℓ is

$$\nu(\Upsilon_{AD} + \Upsilon_R) + (M - 1) \max(\Upsilon_{AD}, \Upsilon_R). \quad (34)$$

The ratio of the computational cost of MISDCQ over that of CISDCQ- ν – i.e., CISDCQ with ν nested iterations on ℓ –, denoted by R_ν , is therefore given by

$$R_\nu := \frac{C_M}{C_C} = \frac{N_M M (\Upsilon_{AD} + \Upsilon_R)}{N_A (\nu(\Upsilon_{AD} + \Upsilon_R) + (M - 1) \max(\Upsilon_{AD}, \Upsilon_R))}. \quad (35)$$

The CISDCQ- ν algorithm reduces the computational cost compared to MISDCQ whenever $R_\nu > 1$. With the introduction of the ratio α as

$$\alpha := \frac{\Upsilon_{AD} + \Upsilon_R}{\max(\Upsilon_{AD}, \Upsilon_R)}, \quad (36)$$

the ratio R_ν comparing the respective computational costs of CISDCQ and MISDCQ simplifies to

$$R_\nu := \frac{N_M}{N_C} \times \frac{\alpha M}{\alpha \nu + M - 1}. \quad (37)$$

We note that $\alpha = 2$ whenever $\Upsilon_{AD} = \Upsilon_R$. In (37), the first ratio compares the convergence of the MISDCQ sweeps with that of the CISDCQ- ν sweeps, while the second ratio compares the computational cost of a single sweep for the two schemes. This decomposition illustrates the two mechanisms leading to a parallel speedup. The first mechanism results from the modification of the update equations (26)-(27) with the introduction of a reaction correction in the diffusion step. It consists in achieving convergence to the fixed-point solution in fewer sweeps with CISDCQ- ν to increase the ratio N_M/N_C . This enhanced convergence rate can be obtained by increasing the number of iterations on ℓ in the nested loop to improve the accuracy of the lagged terms of (26). But, performing more nested iterations is in contradiction to the second mechanism that can be leveraged to reduce the computational cost, which is the reduction of the cost of a single sweep thanks to parallelization to increase the ratio $\alpha M/(\alpha \nu + M - 1)$. This trade-off will be explored with numerical examples in Section 5.

For completeness, we also compare the computational cost of CISDCQ- ν to that of an SDC scheme in which advection is treated explicitly, while diffusion and reaction are treated implicitly in a fully coupled fashion. This scheme, referred to as IMEXQ, is a variant of the IMEX scheme introduced in Minion (2003), and is based on the LU factorization of the integration matrix explained in Section 3.1. The ratio of the computational cost of IMEXQ over that of CISDCQ- ν reads

$$R'_\nu := \frac{N_I}{N_C} \times \frac{\beta M}{\beta \nu + M - 1}, \quad (38)$$

where the coefficient β is defined as

$$\beta := \frac{\Upsilon_{ADR}}{\max(\Upsilon_{AD}, \Upsilon_R)}. \quad (39)$$

where N_I is the number of sweeps needed by IMEXQ to converge to the fixed-point solution, and Υ_{ADR} is the cost of solving the fully coupled advection-diffusion-reaction system. In Section 4, we show that the IMEXQ sweeps converge faster than the CISDCQ- ν and MISDCQ sweeps for stiff problems. But, one expects β to be very large for multidimensional problems with stiff chemistry, since solving the global nonlinear system is expensive and requires efficient physics-based preconditioners for the linear systems.

3.3. Application to low-Mach number combustion

We now describe the application of the CISDCQ time integration scheme to the low-Mach number equation set presented in Section 2. The governing equations are discretized in space using a finite-volume formulation with uniform grid spacing. The fourth-order discretization in space is the same as in Pazner et al. (2016), and relies on the operators found in the finite-volume literature (McCorquodale and Colella, 2011; Zhang et al., 2012). We also use the same volume discrepancy method based on a correction to the divergence constraint. This correction is needed because even if the initial state satisfies the EOS, the variables are updated with fluxes that vary linearly over the time step. Due to the nonlinearity of the EOS, there is no guarantee that each component will evolve in a way that the new state will also satisfy the EOS. The purpose of the δ_χ -correction to the divergence constraint is to adjust the face velocities so that a conservative mass and enthalpy update will end up satisfying the EOS.

For the description of the CISDCQ integration method, we assume that the integration is based on $M + 1$ Gauss-Lobatto nodes, N_C sweeps, and ν iterations on ℓ nested in each sweep. The algorithm to advance the solution from t^n to t^{n+1} is described below.

Initialization

- I1.** Set $(\rho h, \rho \mathbf{Y})^{0,(k)} := (\rho h, \rho \mathbf{Y})^n$ for all $k \in \{0, \dots, N_C\}$, i.e. the solution at temporal node $m = 0$ is a copy of the solution at t^n for all CISDCQ sweeps.
- I2.** Set $(\rho h, \rho \mathbf{Y})^{m,(0)} := (\rho h, \rho \mathbf{Y})^n$ for all $m \in \{1, \dots, M\}$, i.e. the solution for $k = 0$ is a copy of the solution at t^n for all temporal nodes.
- I3.** Define a divergence constraint correction for each temporal interval, $\delta_\chi^{m-1:m,(k)}$, as in Pazner et al. (2016). This correction will be applied to the divergence constraint at each node to ensure consistency with the EOS. Initialize the correction to $\delta_\chi^{m-1:m,(0)} := 0$ for all $m \in \{1, \dots, M\}$.
- I4.** Compute face-averaged velocities at t^n by solving the divergence constraint (7)

$$\nabla \cdot U^n = S^n, \quad (40)$$

which in one dimension can be done by writing $U_{i+1}^n = U_i^n + \int_{x_i}^{x_{i+1}} S$. Then, set $U^{0,(k)} := U^n$ for all $k \in \{0, \dots, N_C\}$. In addition, evaluate the right-hand side of the discretized species and enthalpy equations obtained from (1) and (2), respectively. These terms will be used to evaluate $Q^{0:m+1}[F(\phi^{(0)})]$ in the first CISDCQ sweep.

Sweeps

for $k = 0$ **to** $N_C - 1$ **do**

- S1.** Set $\dot{\omega}^{m,(k+1,0)} := \dot{\omega}^{m,(k)}$ for all $m \in \{0, \dots, M\}$, i.e. the reaction term at iteration $\ell = 0$ at sweep $(k + 1)$ is a copy of the state of the system at the end of sweep (k) . The vector of production terms is $\dot{\omega}^{m,(k+1,0)} = [\dot{\omega}_1^{m,(k+1,0)}, \dots, \dot{\omega}_N^{m,(k+1,0)}]^T$.

for $\ell = 0$ **to** $\nu - 1$ **do**

for $m = 0$ **to** $M - 1$ **do**

- S2.** Update the density $\rho^{m+1,(k+1,\ell+1)}$ explicitly by applying the CISDCQ correction (26) to the discretized continuity equation obtained from (5). Since (5) only contains advection terms, (26) simplifies to

$$\begin{aligned} \rho^{m+1,(k+1,\ell+1)} &= \rho^0 \\ &+ \Delta t \sum_{j=1}^{m-1} \tilde{q}_{m+1,j}^E [-\nabla \cdot (U\rho)^{j,(k+1,\ell+1)} + \nabla \cdot (U\rho)^{j,(k)}] \\ &+ \Delta t \tilde{q}_{m+1,m}^E [-\nabla \cdot (U\rho)^{m,(k+1,\ell)} + \nabla \cdot (U\rho)^{m,(k)}] \\ &+ \Delta t Q^{0:m+1} [-\nabla \cdot (U\rho)^{(k)}], \end{aligned} \quad (41)$$

where the advection flux at substep m and sweep $(k + 1)$ in the third line is lagged in iteration on ℓ .

- S3.** Compute the new mass fractions $Y_{i,AD}^{m+1,(k+1,\ell+1)}$ by applying the CISDCQ correction (26) to the discretized species equation obtained from (1). We write the implicit banded linear system solved with a direct solver during this step as

$$\begin{aligned} (\rho Y_{i,AD})^{m+1,(k+1,\ell+1)} &= (\rho Y_i)^0 + A_{mass} + D_{mass} + R_{mass} \\ &+ \Delta t Q^{0:m+1} [-\nabla \cdot (U\rho Y_i)^{(k)} + \nabla \cdot \Gamma_i^{(k)} + \dot{\omega}_i^{(k)}]. \end{aligned} \quad (42)$$

In the explicit advection correction, A_{mass} , the advection mass flux at substep m and sweep $(k + 1)$ is lagged in iteration on ℓ as follows:

$$\begin{aligned} A_{mass} &= \Delta t \sum_{j=1}^{m-1} \tilde{q}_{m+1,j}^E [-\nabla \cdot (U\rho Y_i)^{j,(k+1,\ell+1)} + \nabla \cdot (U\rho Y_i)^{j,(k)}] \\ &+ \Delta t \tilde{q}_{m+1,m}^E [-\nabla \cdot (U\rho Y_i)^{m,(k+1,\ell)} + \nabla \cdot (U\rho Y_i)^{m,(k)}]. \end{aligned} \quad (43)$$

Similarly, in the implicit diffusion correction, D_{mass} , the diffusion mass flux at substep m and sweep $(k+1)$ is lagged in iteration on ℓ ,

$$\begin{aligned} D_{mass} &= \Delta t \sum_{j=1}^{m-1} \tilde{q}_{m+1,j}^I [\nabla \cdot \Gamma_i^{j,(k+1,\ell+1)} - \nabla \cdot \Gamma_i^{j,(k)}] \\ &\quad + \Delta t \tilde{q}_{m+1,m}^I [\nabla \cdot \Gamma_i^{m,(k+1,\ell)} - \nabla \cdot \Gamma_i^{m,(k)}] \\ &\quad + \Delta t \tilde{q}_{m+1,m+1}^I [\nabla \cdot \Gamma_{i,AD}^{m+1,(k+1,\ell+1)} - \nabla \cdot \Gamma_i^{m+1,(k)}], \end{aligned} \quad (44)$$

where the lagged discrete diffusion flux at substep $m+1$ is

$$\Gamma_{i,AD}^{m+1,(k+1,\ell+1)} := \begin{cases} \rho^{m+1,(k)} \mathcal{D}_i^{m+1,(k)} \nabla Y_{i,AD}^{m+1,(k+1,\ell+1)} & \text{if } \ell = 0 \\ \rho^{m+1,(k+1,\ell)} \mathcal{D}_i^{m+1,(k+1,\ell)} \nabla Y_{i,AD}^{m+1,(k+1,\ell+1)} & \text{otherwise.} \end{cases} \quad (45)$$

Finally, in the implicit reaction correction, R_{mass} , the reaction terms at substeps m and $m+1$ at sweep $(k+1)$ are lagged in iteration on ℓ . The reaction correction is therefore defined as

$$\begin{aligned} R_{mass} &= \Delta t \sum_{j=1}^{m-1} \tilde{q}_{m+1,j}^I [\dot{\omega}_i^{j,(k+1,\ell+1)} - \dot{\omega}_i^{j,(k)}] \\ &\quad + \Delta t \tilde{q}_{m+1,m}^I [\dot{\omega}_i^{m,(k+1,\ell)} - \dot{\omega}_i^{m,(k)}] \\ &\quad + \Delta t \tilde{q}_{m+1,m+1}^I [\dot{\omega}_i^{m+1,(k+1,\ell)} - \dot{\omega}_i^{m+1,(k)}]. \end{aligned} \quad (46)$$

- S4.** Compute the new enthalpy $h_{AD}^{m+1,(k+1,\ell+1)}$ by applying the CISDCQ correction (26) to the discretized energy equation obtained from (2). This step involves using a direct solver to solve the implicit system

$$\begin{aligned} (\rho h_{AD})^{m+1,(k+1,\ell+1)} &= (\rho h)^0 + A_{energy} + D_{energy}^{diff,diff} + D_{energy}^{diff} \\ &\quad + \Delta t Q^{0:m+1} \left[-\nabla \cdot (U \rho h)^{(k)} + \nabla \cdot \frac{\lambda^{(k)}}{c_p^{(k)}} \nabla h^{(k)} + \sum_i \nabla \cdot h_i^{(k)} \left(\Gamma_i^{(k)} - \frac{\lambda^{(k)}}{c_p^{(k)}} \nabla Y_i^{(k)} \right) \right]. \end{aligned} \quad (47)$$

As in the mass fraction update (41), the explicit advection piece in the previous equation, denoted by A_{energy} , is based on a lagged advection flux at substep m and sweep $(k+1)$. Specifically, we write

$$\begin{aligned} A_{energy} &= \Delta t \sum_{j=1}^{m-1} \tilde{q}_{m+1,j}^E \left[-\nabla \cdot (U \rho h)^{j,(k+1,\ell+1)} + \nabla \cdot (U \rho h)^{j,(k)} \right] \\ &\quad + \Delta t \tilde{q}_{m+1,m}^E \left[-\nabla \cdot (U \rho h)^{m,(k+1,\ell)} + \nabla \cdot (U \rho h)^{m,(k)} \right]. \end{aligned} \quad (48)$$

As in Pazner et al. (2016), the differential diffusion terms corresponding to the sum in the right-hand side of (2) are evaluated explicitly to simplify the linear system that needs to be solved. Therefore, the differential diffusion correction, $D_{energy}^{diff,diff}$, is

$$\begin{aligned} D_{energy}^{diff,diff} &= \Delta t \sum_{j=1}^{m-1} \tilde{q}_{m+1,j}^E \left[\sum_i \nabla \cdot h_i^{j,(k+1,\ell+1)} \left(\Gamma_i^{j,(k+1,\ell+1)} - \frac{\lambda^{j,(k+1,\ell+1)}}{c_p^{j,(k+1,\ell+1)}} \nabla Y_i^{j,(k+1,\ell+1)} \right) \right. \\ &\quad \left. - \nabla \cdot h_i^{j,(k)} \left(\Gamma_i^{j,(k)} - \frac{\lambda^{j,(k)}}{c_p^{j,(k)}} \nabla Y_i^{j,(k)} \right) \right] \\ &\quad + \Delta t \tilde{q}_{m+1,m}^E \left[\sum_i \nabla \cdot h_i^{m,(k+1,\ell)} \left(\Gamma_i^{m,(k+1,\ell)} - \frac{\lambda^{m,(k+1,\ell)}}{c_p^{m,(k+1,\ell)}} \nabla Y_i^{m,(k+1,\ell)} \right) \right. \\ &\quad \left. - \nabla \cdot h_i^{m,(k)} \left(\Gamma_i^{m,(k)} - \frac{\lambda^{m,(k)}}{c_p^{m,(k)}} \nabla Y_i^{m,(k)} \right) \right]. \end{aligned} \quad (49)$$

Following the approach of (44), the diffusion correction, D_{energy}^{diff} , contains a lagged diffusion flux at substep m and sweep $(k+1)$

$$\begin{aligned}
 D_{energy}^{diff} = & \Delta t \sum_{j=1}^{m-1} \tilde{q}_{m+1,j}^I \left[\nabla \cdot \frac{\lambda^{j,(k+1,\ell+1)}}{c_p^{j,(k+1,\ell+1)}} \nabla h^{j,(k+1,\ell+1)} - \nabla \cdot \frac{\lambda^{j,(k)}}{c_p^{j,(k)}} \nabla h^{j,(k)} \right] \\
 & + \Delta t \tilde{q}_{m+1,m}^I \left[\nabla \cdot \frac{\lambda^{m,(k+1,\ell)}}{c_p^{m,(k+1,\ell)}} \nabla h^{m,(k+1,\ell)} - \nabla \cdot \frac{\lambda^{m,(k)}}{c_p^{m,(k)}} \nabla h^{m,(k)} \right] \\
 & + \Delta t \tilde{q}_{m+1,m+1}^I \left[\nabla \cdot \left(\frac{\lambda}{c_p} \right)_{AD}^{m+1,(k+1,\ell+1)} \nabla h_{AD}^{m+1,(k+1,\ell+1)} - \nabla \cdot \frac{\lambda^{m+1,(k)}}{c_p^{m+1,(k)}} \nabla h^{m+1,(k)} \right],
 \end{aligned} \tag{50}$$

where the diffusion coefficient at substep $m+1$, denoted by $(\lambda/c_p)_{AD}^{m+1,(k+1,\ell+1)}$, is lagged using the same method as in (45). After the enthalpy update, we can set

$$(\rho h)^{m+1,(k+1,\ell+1)} = \rho^{m+1,(k+1,\ell+1)} h_{AD}^{m+1,(k+1,\ell+1)}, \tag{51}$$

since there is no contribution due to reactions in the enthalpy update. If $\ell = 0$, recompute the diffusion terms in the right-hand side of the discrete species and energy equations. Following (28)-(29), these terms will be used to define the quantities evaluated at $m+1, (k+1, 0)$ at the next iteration $\ell = 1$.

- S5.** Compute the new mass fractions $Y_i^{m+1,(k+1,\ell+1)}$ by applying the CISDCQ correction (31) to the discretized species equation

$$\begin{aligned}
 (\rho Y_i)^{m+1,(k+1,\ell+1)} = & \rho^{m+1,(k+1,\ell+1)} Y_{i,AD}^{m+1,(k+1,\ell+1)} \\
 & + \Delta t \tilde{q}_{m+1,m}^I \left[\dot{\omega}_i^{m,(k+1,\ell+1)} - \dot{\omega}_i^{m,(k+1,\ell)} \right] \\
 & + \Delta t \tilde{q}_{m+1,m+1}^I \left[\dot{\omega}_i^{m+1,(k+1,\ell+1)} - \dot{\omega}_i^{m+1,(k+1,\ell)} \right].
 \end{aligned} \tag{52}$$

To obtain the new mass fractions from (52), we form the backward-Euler type nonlinear system

$$\rho^{m+1,(k+1,\ell+1)} \mathbf{Y} - \Delta t \tilde{q}_{m+1,m+1}^I \dot{\boldsymbol{\omega}}^{m+1,(k+1,\ell+1)}(\mathbf{Y}) = \mathbf{b}, \tag{53}$$

where we defined a right-hand side \mathbf{b} obtained from (52). The density and the enthalpy have been computed in the previous steps of the algorithm and are known. The system is solved with Newton's method in which the initial guess is the solution at the previous nested iteration on ℓ . The Jacobian matrix is computed analytically (Perini et al., 2012).

- S6.** Increment the divergence constraint correction by setting

$$\delta_\chi^{m:m+1,(k+1,\ell+1)} := \delta_\chi^{m:m+1,(k)} + \frac{2}{p_0} \left(\frac{p_{EOS}^{m+1,(k+1,\ell+1)} - p_0}{\Delta t^m} \right), \tag{54}$$

where the thermodynamic pressure, p_{EOS} , is defined in (4). Then, solve the divergence constraint (7)

$$\nabla \cdot U^{m+1,(k+1,\ell+1)} = S^{m+1,(k+1,\ell+1)} + \delta_\chi^{m:m+1,(k+1,\ell+1)}. \tag{55}$$

Finally, recompute the diffusion terms in the right-hand side of the species and enthalpy equations (1)-(2).

end for (end loop over temporal nodes m)

end for (end loop over nested iterations ℓ)

S7. Set $(\rho\mathbf{Y}, \rho h)^{m, (k+1)} := (\rho\mathbf{Y}, \rho h)^{m, (k+1, \nu)}$, i.e., we save the solution at the last iteration ν of sweep $(k+1)$.

end for (end loop over CISDCQ sweeps k)

We highlight that by construction, steps **S2**, **S3**, and **S4** at node $m+1, (k+1, \ell+1)$ can be executed without knowing the state of the system at $m, (k+1, \ell+1)$ thanks to the decoupling method based on lagging (see Section 3.2). Therefore, if enough processors are available, a given processor executes task \mathcal{T}_1 , i.e., it performs the advection and diffusion steps, **S2**, **S3**, and **S4**, at $m+1, (k+1, 1)$ while another processor computes task \mathcal{T}_2 corresponding to the reaction step and right-hand side update (**S5** and **S6**) at $m, (k+1, 1)$. If more iterations on ℓ are used, the pipelining strategy sketched in Fig. 2 is used. The accuracy and efficiency of the numerical methodology for low-Mach number combustion will be assessed with a flame simulation in Section 5.

4. Convergence of the SDC sweeps

A key property of all SDC-based methods is their convergence with iteration to the collocation solution used to advance each time step. This is to be distinguished from the *convergence* (in the more traditional sense) of the temporal discretization with decreasing time step size. In this section, we explore the former using a parameterized linear model problem, which allows us to demonstrate the behavior of the time stepping scheme in the various limits of competing stiffnesses between the advection, diffusion and reaction components of the system. A simple model problem for this purpose is given by the ODE

$$\begin{cases} \phi'(t) &= a\phi(t) + d\phi(t) + r\phi(t), & a, d, r \in \mathbb{R} \\ \phi(0) &= \phi^0, \end{cases} \quad (56)$$

where a , d , and r represent advection, diffusion, and reaction processes, respectively. In order to quantify the convergence of the sweeps, we recast the generalized update equations (26)-(27) into an iteration matrix for CISDCQ (and similarly for MISDC and MISDCQ), and we analyze the spectrum of this matrix.

In matrix notation, the approximate solutions obtained with CISDCQ at the end of sweep $(k+1)$ are denoted by $\Phi^{(k+1)} = [\phi^{1, (k+1)}, \dots, \phi^{M, (k+1)}]^T \in \mathbb{R}^M$. This vector is computed iteratively using ν successive nested iterations on ℓ applied to the M substeps of the temporal interval. For $m \in \{0, \dots, M-1\}$ and $\ell \in \{0, \dots, \nu-1\}$, the intermediate solutions at nested iteration $\ell+1$, after substep $m+1$, are stored in the vector

$$\Phi_{m+1}^{(k+1, \ell+1)} := [\phi^{1, (k+1, \ell+1)}, \dots, \phi^{m+1, (k+1, \ell+1)}, 0, \dots, 0]^T \in \mathbb{R}^M. \quad (57)$$

The vector $\Phi_{AD, m+1}^{(k+1, \ell+1)}$ storing the intermediate solutions after the diffusion update is defined analogously. In Appendix A, we use the matrix form of the update equations (26)-(27) to show by induction on m and ℓ that the following relationship holds for all $m \in \{0, \dots, M-1\}$ and $\ell \in \{0, \dots, \nu-1\}$:

$$\begin{aligned} \Phi_{m+1}^{(k+1, \ell+1)} &= \mathbf{M}_{1, m+1}^{(\ell+1)} [\phi^0 \mathbf{1} + s\Delta t \phi^0 \mathbf{q} + \Delta t (s\tilde{\mathbf{Q}} - a\tilde{\mathbf{Q}}^E - (d+r)\tilde{\mathbf{Q}}^I) \Phi^{(k)}] \\ &+ \mathbf{M}_{2, m+1}^{(\ell+1)} \Phi^{(k)}, \end{aligned} \quad (58)$$

where $s = a + d + r$. The matrices $\mathbf{M}_{1, m+1}^{(\ell+1)}, \mathbf{M}_{2, m+1}^{(\ell+1)} \in \mathbb{R}^{M \times M}$ depend on the matrices $\tilde{\mathbf{Q}}, \tilde{\mathbf{Q}}^I$, and $\tilde{\mathbf{Q}}^E$, on the scalars $m, \ell, \Delta t, a, d$, and r , and can be computed iteratively as explained in the Appendix. The vector \mathbf{q} is the first column of the matrix \mathbf{Q} defined by (24). Assuming that the scheme is based on $M+1$ temporal nodes and ν nested iterations on ℓ , (58) yields an expression of $\Phi^{(k+1)}$ as a function of the previous iterate, $\Phi^{(k)}$, given by

$$\begin{aligned} \Phi^{(k+1)} &= \Phi_M^{(k+1, \nu)} = \mathbf{M}_{1, M}^{(\nu)} [\phi^0 \mathbf{1} + s\Delta t \phi^0 \mathbf{q} + \Delta t (s\tilde{\mathbf{Q}} - a\tilde{\mathbf{Q}}^E - (d+r)\tilde{\mathbf{Q}}^I) \Phi^{(k)}] \\ &+ \mathbf{M}_{2, M}^{(\nu)} \Phi^{(k)}. \end{aligned} \quad (59)$$

Taking the difference between two consecutive iterates in (59), we obtain

$$\Phi^{(k+1)} - \Phi^{(k)} = \mathbf{G}(\Phi^{(k)} - \Phi^{(k-1)}). \quad (60)$$

The iteration matrix, $\mathbf{G} \in \mathbb{R}^{M \times M}$, is defined as

$$\mathbf{G} := \mathbf{M}_{1,M}^{(\nu)} \Delta t (s\tilde{\mathbf{Q}} - a\tilde{\mathbf{Q}}^E - (d+r)\tilde{\mathbf{Q}}^I) + \mathbf{M}_{2,M}^{(\nu)}. \quad (61)$$

We compare the properties of the CISDCQ iteration matrix with those of MISDCQ and IMEXQ. We reiterate that the IMEXQ scheme is used to illustrate the convergence of the spectral correction process when advection is treated explicitly while diffusion and reaction are treated implicitly in a fully coupled fashion. Using these results, we analyze the correction process, which is convergent if and only if the spectral radius of the iteration matrix \mathbf{G} is strictly smaller than one, that is

$$\gamma(\mathbf{G}) < 1. \quad (62)$$

In Fig. 3, we first compute the spectral radius of the iteration matrix while keeping the ratio d/r fixed. With this approach, we evaluate the asymptotic convergence rate of the schemes when the diffusion and reaction terms become stiff simultaneously. We assume a fixed unit time step size $\Delta t = 1$, and we use Gauss-Lobatto nodes. When the problem is not stiff ($|r| < 1$), the advection term dominates and all the schemes, including IMEXQ, converge in sweeps to the fixed-point solution at the same asymptotic rate. When the problem becomes very stiff ($|r| > 10^3$), the IMEXQ sweeps retain a fast convergence rate and one can show that $\lim_{(d+r) \rightarrow -\infty} \gamma(\mathbf{G}) = 0$ (see Weiser (2015)). But, this property does not hold when the diffusion and reaction updates are computed in two separate steps. Therefore, the asymptotic convergence rate of the MISDCQ and CISDCQ sweeps deteriorates significantly for large negative values of d and r . Finally, for intermediate values of r ($1 \leq |r| \leq 10^3$), we observe that the number of nested iterations on ℓ has a strong impact on the asymptotic convergence rate of CISDCQ. If only one nested iteration on ℓ is used, the CISDCQ-1 sweeps converge slightly slower than with MISDCQ. However, with respectively three and six nested iterations, the CISDCQ-3 and CISDCQ-6 sweeps converge faster than with MISDCQ. In particular, the CISDCQ-6 sweeps achieve the same convergence rate as IMEXQ for a relatively larger fraction of the parameter space.

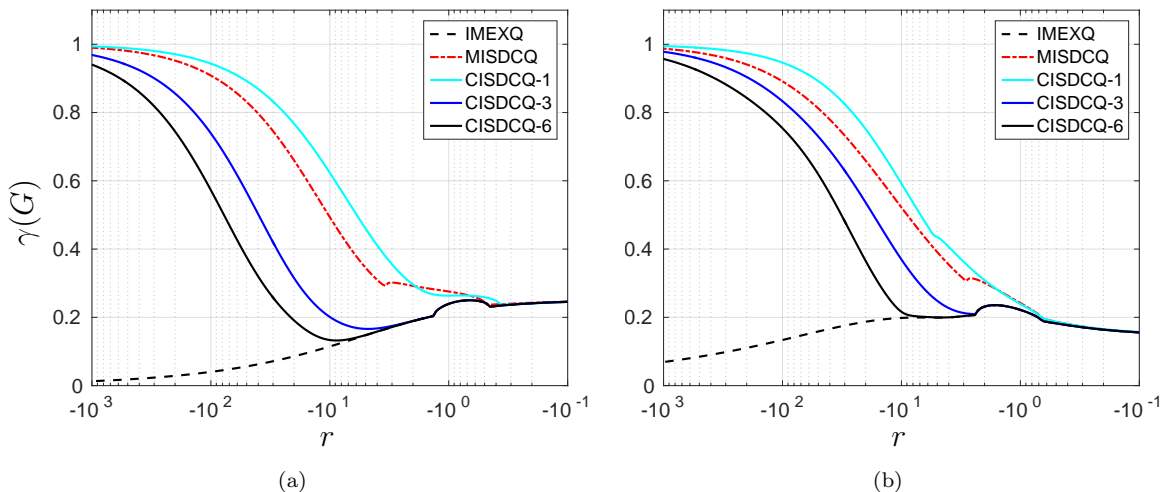


Figure 3: Spectral radius of the iteration matrix, \mathbf{G} , as a function of the reaction coefficient, r . The advection and diffusion coefficients are set to $a = 1$ and $d = r/2$, respectively. In 3(a), three Gauss-Lobatto nodes are used, whereas in 3(b), five Gauss-Lobatto nodes are used.

In Fig. 4, we explore another dimension of the parameter space. We compute the spectral radius of \mathbf{G} while keeping the diffusion coefficient d constant and varying the ratio d/r to evaluate the asymptotic convergence rate of the sweeps when the reaction term strongly dominates the diffusion term, or conversely vanishes. We still assume that the time step size is constant, equal to one. We observe that with all

the schemes, the sweeps converge at the same rate when the reaction term vanishes ($|r| \leq 1$), in which case (56) reduces to an advection-diffusion problem. But, if $|r|$ is increased with a constant diffusion strength, increasing the number of nested iterations on ℓ improves the convergence rate of the sweeps, even when the problem is very stiff ($|r| \geq 10^3$). In this configuration, the CISDCQ-1 sweeps still do not converge as fast as the MISDCQ sweeps. But, CISDCQ-3 and CISDCQ-6 converge in sweeps faster than the reference scheme.

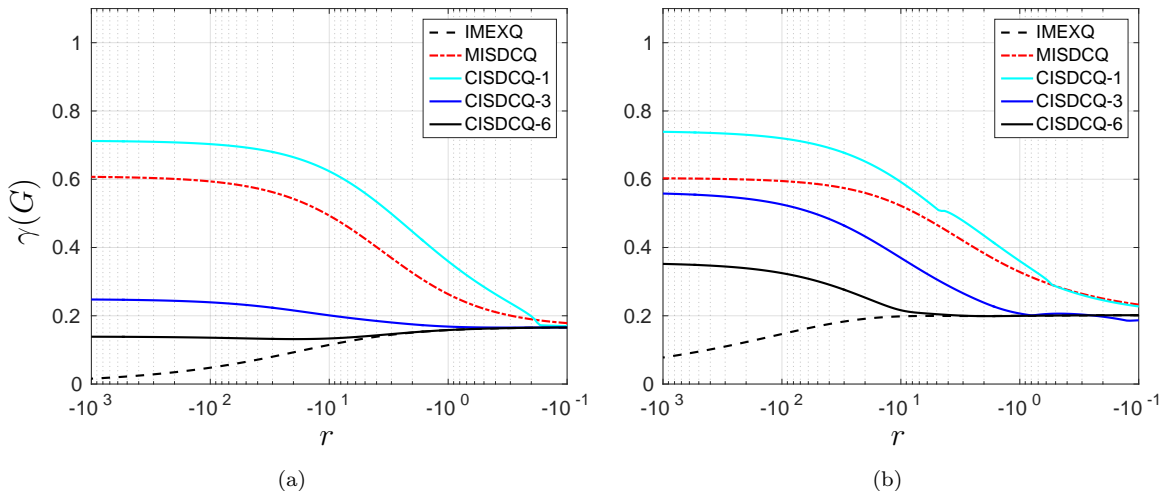


Figure 4: Spectral radius of the iteration matrix, \mathbf{G} , as a function of the reaction coefficient, r . The advection and diffusion coefficients are set to $a = 1$ and $d = -5$, respectively. In 4(a), three Gauss-Lobatto nodes are used, whereas in 4(b), five Gauss-Lobatto nodes are used.

5. Numerical examples

For simplicity, we assess the reduction in computational cost obtained with CISDCQ using (37). This provides a fair comparison between the time integration methods while using a serial code to simulate parallelism in CISDCQ. The implementation of a truly parallel version of CISDCQ on a shared-memory platform is a non-trivial task left for future work.

5.1. Validation of convergence analysis – Linear model

Next, we confirm the analysis above by evolving the linear model problem (56) with the initial condition $\phi^0 = 1$, for several representative values of the stiffness parameters, a , d , and r . For these cases, we discretize the temporal interval $\Delta t = 1$ with five Gauss-Lobatto nodes ($M = 4$). We keep the advection coefficient constant equal to $a = 1$ and we vary the diffusion and reaction coefficients $d, r \in \mathbb{R}^-$ to assess the stability and convergence rate of the CISDCQ scheme when the problem becomes very stiff. We reiterate here that performing the 2ν pipelined tasks involved in CISDCQ- ν requires up to $\max(2\nu, M)$ processors working in parallel. Given that $M = 4$ in this section, the CISDCQ-1, CISDCQ-3, and CISDCQ-6 schemes use respectively up to 2, 4, and still 4 processors to compute the solution.

Following the approach of Section 4, we first fix the ratio $r/d = 2$ and increase the absolute value of the coefficients d and r at the same rate. Fig. 5 shows the convergence rate of the difference between two iterates, $|\phi^{M,(k+1)} - \phi^{M,(k)}|$, as a function of the number of sweeps for $r = -4, -20, -100$. In each case, the convergence rate of this quantity is consistent with the analysis of Section 4. Specifically, for the non-stiff problem of Fig. 5(a), the CISDCQ-1 sweeps converge at a slower rate than those of MISDCQ, whereas the CISDCQ-3 and CISDCQ-6 sweeps converge slightly faster than those of MISDC and MISDCQ. As the problem becomes stiffer in Figs. 5(b) and 5(c), CISDCQ-3 and CISDCQ-6 converge in sweeps significantly faster than MISDC and MISDCQ. We also note that for the stiff cases, performing six nested iterations on ℓ instead of three produces a faster convergence of the CISDCQ sweeps. However, increasing the number of nested iterations beyond three does not necessarily improve the efficiency of CISDCQ, as shown by the

ratio R_ν computed with (37) and the assumption that $\Upsilon_{AD} = \Upsilon_R$. Considering the number of sweeps necessary to achieve $|\phi^{M,(k+1)} - \phi^{M,(k)}| \leq 10^{-14}$, the values of R_ν for each configuration are in Table 1.

r	$R_{\nu=1}$	$R_{\nu=3}$	$R_{\nu=6}$
-4	1.4	1.5	0.9
-20	1.1	2.6	1.6
-100	0.9	1.8	2.0

Table 1: Ratio of the computational cost of MISDCQ over that of CISDCQ- ν for the linear model problem (56) with $a = 1$ and a fixed ratio $r/d = 2$.

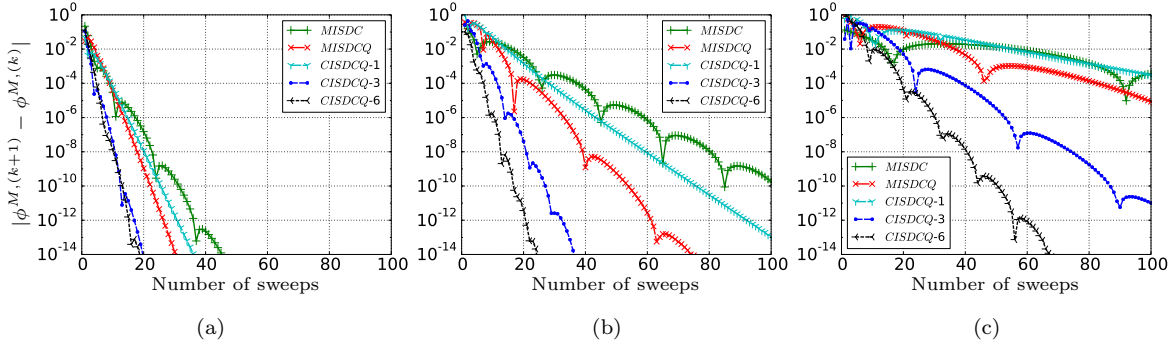


Figure 5: Convergence of $|\phi^{M,(k+1)} - \phi^{M,(k)}|$ as a function of the number of sweeps for the linear model problem (56) with $\phi^0 = 1$ and $a = 1$. The diffusion and reaction coefficients are set to $d = -2, r = -4$ in 5(a), $d = -10, r = -20$ in 5(b), and $d = -50, r = -100$ in 5(c).

Next, we study the computational cost of CISDCQ for multiple ratios r/d to make sure that the scheme remains stable when the diffusion term dominates the reaction term, and vice-versa. The convergence of $|\phi^{M,(k+1)} - \phi^{M,(k)}|$ as a function of the number of sweeps for these cases is in Fig. 6. The CISDCQ-3 and CISDCQ-6 sweeps converge faster than those of MISDCQ when the absolute magnitude of the diffusion term is 20 times larger than that of the reaction term ($d = -100, r = -5$) in Fig. 6(a), when the two terms have the same magnitude ($d = r = -5$) in Fig. 6(b), and when the absolute magnitude of the diffusion term is 20 times smaller than that of the reaction term ($d = -5, r = -100$) in Fig. 6(c). We observe again that increasing the number of nested iterations on ℓ beyond three accelerates the convergence of the sweeps but can degrade the reduction in computational cost obtained with CISDCQ. The ratio R_ν for a tolerance of 10^{-14} is in Table 2. This highlights the need for an adaptive mechanism to select the optimal number of nested iterations on ℓ at each sweep based on the stiffness of the problem, the number of SDC nodes, and the number of available processors. Such a strategy would in particular stop the nested iterations before the CISDCQ performance starts degrading. This will be explored in future work.

d	r	$R_{\nu=1}$	$R_{\nu=3}$	$R_{\nu=6}$
-100	-5	1.0	1.2	1.2
-5	-5	2.1	1.5	1.1
-5	-100	1.1	1.6	1.4

Table 2: Ratio of the computational cost of MISDCQ over that of CISDCQ- ν for the linear model problem (56) with $a = 1$ and multiple values of the ratio r/d .

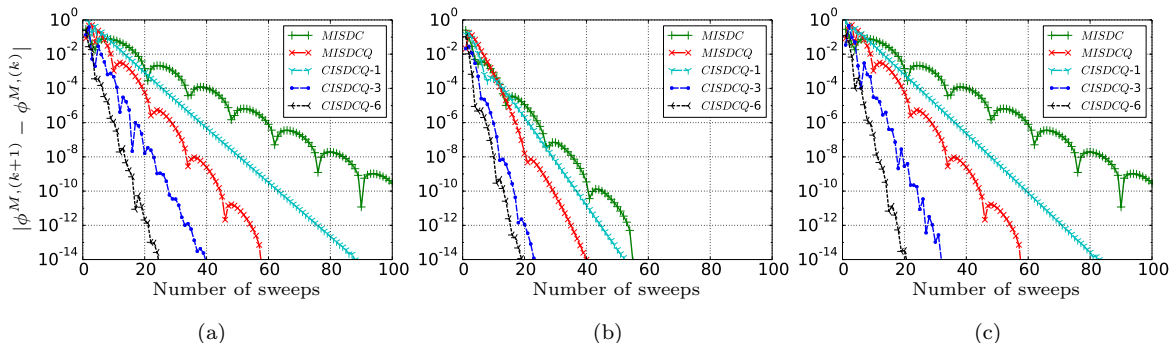


Figure 6: Convergence of $|\phi^{M,(k+1)} - \phi^{M,(k)}|$ as a function of the number of sweeps for the linear model problem (56) with $\phi^0 = 1$ and $a = 1$. The diffusion and reaction coefficients are set to $d = -100$, $r = -5$ in 6(a), $d = -5$, $r = -5$ in 6(b), and $d = -5$, $r = -100$ in 6(c).

5.2. Nonlinear test PDE

It is instructive to verify that the results of the previous section can predict reasonably well the performance of CISDCQ on a more complex nonlinear coupled problem. The one-dimensional advection-diffusion-reaction model,

$$\begin{cases} \phi_t(x, t) &= a\phi_x + d\phi_{xx} + r\phi(\phi - 1)(\phi - 1/2) & \text{for } (x, t) \in [0, 20] \times [0, T], \\ \phi(0, t) &= 1, \\ \phi(20, t) &= 0, \\ \phi(x, 0) &= \phi^0(x), \end{cases} \quad (63)$$

captures many of the generic features and coupling of the low-Mach combustion system, yet avoids complexities associated with parameterized equations of state, transport properties, and reaction physics. A suitable initial condition is given by

$$\phi^0(x) = \frac{1}{2}(1 + \tanh(20 - 2x)). \quad (64)$$

This PDE is solved with the method of lines based on a finite-volume approach. The advection term is discretized using a fourth-order operator, $A(\phi)$, and the diffusion term is approximated with a fourth-order Laplacian operator, $D(\phi)$. This discretization scheme leads to the nonlinear system of ODEs

$$\phi_t = A(\phi) + D(\phi) + R(\phi), \quad (65)$$

where $R(\phi) = r\phi(\phi - 1)(\phi - 1/2)$ denotes the reaction term. This system is solved with the MISDC, MISDCQ, and CISDCQ schemes based on five Gauss-Lobatto nodes to compare their accuracy and number of sweeps needed to achieve convergence to the fixed-point solution. As in the previous section, CISDCQ-1, CISDCQ-3, and CISDCQ-6 allow to use respectively up to 2, 4, and 4 parallel processors.

We first perform a refinement study in time to assess the accuracy of CISDCQ. We verify that each CISDCQ sweep increases the temporal order of accuracy by one for mildly stiff problems. To this end, we refine the time step size while keeping the grid spacing fixed to $\Delta x = 0.1$ ($n_x = 200$). We set the coefficients in (63) to $a = 1$, $d = 2$, and $r = 4$. Here, the error is quantified using the L_1 -norm

$$\|\phi - \phi^{ref}\|_1 = \frac{1}{n_x} \sum_{i=1}^{n_x} |\phi(x_i, t_{final}) - \phi^{ref}(x_i, t_{final})|, \quad (66)$$

where n_x is the number of cells and ϕ (respectively, ϕ^{ref}) denotes the approximate solution (respectively, the averaged reference solution). The results are compared to a reference solution generated with MISDCQ for $\Delta t_{ref} = \Delta x/32 = 0.003125$, which corresponds to an advective CFL number of $\sigma_{ref} = 0.03125$. Fig. 7 shows the L_1 -norm of the error with respect to the reference solution as a function of the time step

size. The error obtained with CISDCQ-1 – i.e., the CISDCQ scheme based on only one nested iteration on ℓ – decreases at the same rate as with MISDC and MISDCQ when the time step size is reduced. Specifically, CISDCQ-1 achieves second-order accuracy with two sweeps, and fourth-order accuracy with four sweeps. With eight sweeps, the asymptotic range is not reached and the three schemes only exhibit a seventh-order accuracy. The results obtained with CISDCQ-3 and CISDCQ-6, based on three and six nested iterations, respectively, are similar to those of CISDCQ-1 and are therefore not presented.

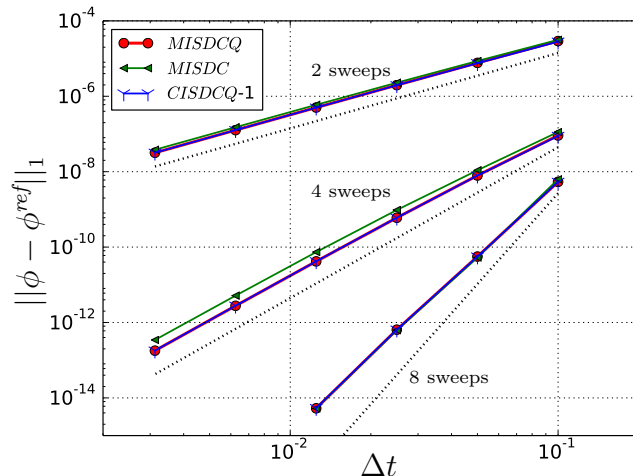


Figure 7: L_1 -error of the MISDC, MISDCQ, and CISDCQ-1 solutions with respect to the reference solution as a function of time for the nonlinear test PDE (63) with $a = 1$, $d = 2$, $r = 4$. The dashed lines indicate the theoretical order of accuracy of the MISDC-type schemes. The solid lines corresponding to the MISDCQ and CISDCQ-1 schemes are on top of each other.

Next, we consider a single time step and we investigate the convergence of the iterative spectral deferred correction process for different levels of stiffness as in Section 5.1. The spatial discretization is still based on $n_x = 200$ cells and the time step is fixed to $\Delta t = \Delta x/2 = 0.05$. The advection coefficient is still set to $a = 1$, which corresponds to an advective CFL number of $\sigma = 1/2$. We consider three cases with increasingly large value of the diffusion and reaction coefficients d and r . The convergence of the L_1 -norm of the difference between two iterates, $\|\phi^{M,(k+1)} - \phi^{M,(k)}\|_1$, as a function of the number of sweeps for the first time step of the simulation is in Fig. 8.

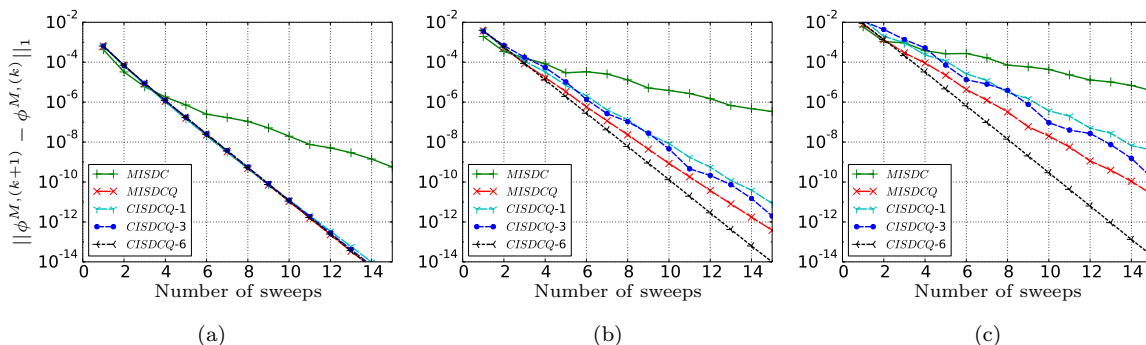


Figure 8: Convergence of $\|\phi^{M,(k+1)} - \phi^{M,(k)}\|_1$ as a function of the number of sweeps for the nonlinear test PDE (63) with $a = 1$. The diffusion and reaction coefficients are set to $d = 2$, $r = 4$ in 8(a), $d = 8$, $r = 16$ in 8(b), and $d = 16$, $r = 32$ in 8(c).

To evaluate the computational cost of CISDCQ- ν after 15 sweeps, we first compute the value $\epsilon \in \mathbb{R}^+$ such that $\|\phi^{M,(15)} - \phi^{M,(14)}\|_1 = \epsilon$, where $\phi^{M,(14)}$ and $\phi^{M,(15)}$ are the approximate solutions generated by MISDCQ after 14 and 15 sweeps, respectively. Then, we compute the number of sweeps N_C necessary to

achieve $\|\phi^{M,(N_C)} - \phi^{M,(N_C-1)}\|_1 \leq \epsilon$ with CISDCQ- ν . Finally, using (37) and the assumption that $\Upsilon_{AD} = \Upsilon_R$, we compute the ratio R_ν for the CISDCQ- ν integration scheme as $R_\nu = 15/N_C \times 2M/(2\nu + M - 1)$. The results can be found in Table 3.

In Fig. 8(a), the sweeps of the integration methods based on the LU decomposition of the integration matrix, namely, MISDCQ and CISDCQ, converge at the same rate. The MISDC sweeps converge significantly slower and this scheme requires almost twice as many sweeps to achieve $\|\phi^{M,(k+1)} - \phi^{M,(k)}\|_1 \leq 10^{-11}$. For this mildly stiff problem, increasing the number of iterations on ℓ in the nested loop does not accelerate the convergence of the CISDCQ sweeps. Therefore, it is more advantageous to use CISDCQ-1 – i.e., only one iteration in the nested loop –, which has a computational cost ratio of $R_{\nu=1} = 1.6$ when $d = 2$ and $r = 4$. In CISDCQ-3 and CISDCQ-6, the overhead caused by the nested loop is not compensated for by an enhanced convergence of the sweeps, which is why we only obtain $R_{\nu=3} \approx 0.9$ and $R_{\nu=6} \approx 0.5$ for $d = 2$ and $r = 4$.

But, in Figs. 8(b) and 8(c), we clearly see that the nested iterations on ℓ have a positive impact on the convergence of the CISDCQ-3 and CISDCQ-6 sweeps when the problem becomes stiffer. For instance, the convergence of the CISDCQ-1 sweeps deteriorates significantly when d and r increase, whereas that of CISDCQ-6 is not affected by the stronger stiffness of the problem. However, this enhanced convergence of the CISDCQ-3 and CISDCQ-6 sweeps is not sufficient to yield a significant reduction in computational cost. In fact, in these two configurations, it is still more efficient to use CISDCQ-1 to reduce the cost, as shown by the values of R_ν . We obtain $R_{\nu=1} \approx 1.4$, $R_{\nu=3} \approx 0.8$, and $R_{\nu=6} \approx 0.6$ for $d = 8$ and $r = 16$. When $d = 16$ and $r = 32$, we achieve $R_{\nu=1} \approx 1.2$, $R_{\nu=3} \approx 0.7$, and $R_{\nu=6} \approx 0.7$. As in the previous example, an adaptive strategy to stop the nested iterations before R_ν starts decreasing would considerably benefit the CISDCQ algorithm.

d	r	$R_{\nu=1}$	$R_{\nu=3}$	$R_{\nu=6}$
2	4	1.6	0.9	0.5
8	16	1.4	0.8	0.6
16	32	1.2	0.7	0.7

Table 3: Ratio of the computational cost of MISDCQ over that of CISDCQ- ν for the nonlinear test PDE (63) with $a = 1$ and multiple values of d and r .

5.3. Dimethyl Ether Flame

In this section, we assess the performance of CISDCQ using a one-dimensional unsteady simulation of a premixed flame based on a 39-species, 175-reaction dimethyl ether (DME) chemistry mechanism (Bansal et al., 2015). This example is challenging for the SDC schemes discussed in this work because the DME chemistry mechanism is very stiff. The system is evolved on the relatively slow advection time scale to evaluate the ability of the schemes to capture the nonlinear coupling between the faster diffusion and reaction processes. The domain length is $d = 0.6$ cm. The inlet stream at $T = 298$ K, $p = 1$ atm, has composition, $\mathbf{Y}(\text{CH}_3\text{OCH}_3 : \text{O}_2 : \text{N}_2) = (0.0726 : 0.2160 : 0.7114)$, obtained from the one-dimensional solution computed with the PREMIX package (Kee et al., 1985). We arbitrarily set the inlet velocity to $5 \text{ cm}\cdot\text{s}^{-1}$. The initial pressure in the domain is constant, equal to 1 atm. The initial mixture composition is also constant, equal to the inlet stream composition given above. Finally, the initial temperature field is set to

$$T(x) = T_{\min} + (T_{\max} - T_{\min}) \exp \left[-\frac{1}{2} \left(\frac{x - d/2}{\kappa} \right)^2 \right] \quad x \in [0, 0.6], \quad (67)$$

with $T_{\min} = 298$ K, $T_{\max} = 1615$ K, and $\kappa = 0.0275$. We simulate this test case using a constant time step size subdivided with three Gauss-Lobatto nodes. We note that with this small number of SDC nodes ($M = 2$), we use up to two processors to perform the 2ν pipelined tasks employed by CISDCQ- ν . That is, CISDCQ-2, CISDCQ-3, and CISDCQ-4 all allow to use two processors working in parallel.

We first make sure that the CISDCQ scheme has the same order of accuracy as MISDCQ upon refinement in space and time. This is shown in Table 4, in which we perform a refinement study for a fixed

advective CFL number of $\sigma \approx 0.65$, starting from $n_x = 128$ and $\Delta t = 4 \times 10^{-6}$ s. The system is evolved for 8.8×10^{-5} s. The reference solution is obtained with MISDCQ with $n_x = 1024$ and $\Delta t = 5 \times 10^{-7}$ s. The schemes are tested with eight sweeps per time step, as in Pazner et al. (2016). Table 4 demonstrates that MISDCQ and CISDCQ-2 have the same order of accuracy for the main thermodynamic variables as well as for the mass fraction of dioxygen. This shows that CISDCQ is as accurate as MISDCQ even when a relatively small number of nested iterations on ℓ is used. For this extremely stiff example, the MISDC sweeps fail to converge. The MISDC scheme is therefore significantly less accurate than MISDCQ and CISDCQ-2. The same is true for CISDCQ-1, whose results are therefore not included in Table 4. We note that for the initial setup (67) and the levels of spatio-temporal refinement used here, none of the schemes is in the asymptotic convergence regime, and more sweeps would be required to reach the formal order of accuracy of the schemes. This is why MISDCQ and CISDCQ-2 do not achieve fourth-order accuracy even though the spatial and temporal discretizations are formally fourth-order accurate.

	Variable	L_1^{128}	$r^{128/256}$	L_1^{256}	$r^{256/512}$	L_1^{512}
MISDC	Y_{O_2}	2.62E-03	1.05	1.26E-03	0.34	1.00E-03
	ρ	1.15E-05	0.87	6.29E-06	0.31	5.07E-06
	ρh	6.99E+04	0.86	3.84E+04	0.31	3.11E+04
	T	2.86E+01	0.92	1.51E+01	0.31	1.21E+01
MISDCQ	Y_{O_2}	8.91E-04	2.42	1.67E-04	2.27	3.45E-05
	ρ	4.61E-06	2.33	9.19E-07	2.25	1.93E-07
	ρh	2.78E+04	2.33	5.51E+03	2.26	1.15E+03
	T	1.07E+01	2.37	2.08E+00	2.27	4.32E-01
CISDCQ-2	Y_{O_2}	8.89E-04	2.42	1.66E-04	2.27	3.44E-05
	ρ	4.60E-06	2.32	9.18E-07	2.25	1.92E-07
	ρh	2.77E+04	2.33	5.50E+03	2.25	1.15E+03
	T	1.07E+01	2.36	2.07E+00	2.26	4.32E-01

Table 4: L_1 -norm of the error with respect to the reference solution as a function of the level of space-time refinement for the DME flame simulation. For brevity, this table only reports the mass fraction Y_{O_2} , but similar results are observed for the other species in the system. The convergence rate is defined as $r^{c/f} = \log_2(L_1^c/L_1^f)$.

In Fig. 9, we evaluate the magnitude of the thermodynamic drift as a function of the level of space-time refinement for the different schemes. To evaluate the magnitude of the drift, we use the L_∞ -norm

$$\|p_{EOS} - p_0\|_\infty = \max_{i \in \{1, \dots, n_x\}} (|p_{EOS}(x_i, t_{final}) - p_0|), \quad (68)$$

where the thermodynamic pressure, p_{EOS} , is defined in (4). We still use a constant time step size corresponding to a CFL number $\sigma \approx 0.65$ and eight sweeps per time step. For this problem, MISDC yields a thermodynamic drift that is multiple orders of magnitude larger than that of the MISDCQ and CISDCQ schemes. MISDCQ and CISDCQ-2 achieve a similar thermodynamic drift for all levels of refinement, which is consistent with the results of Table 4. Increasing the number of nested iterations on ℓ yields a smaller norm of the drift. Specifically, CISDCQ-3 and CISDCQ-4 produce mass and energy fields that are more consistent with the EOS for the coarse levels of refinement ($n_x = 128, 256$).

Finally, we assess the convergence of the correction process in the last time step of the DME flame simulation, for a level of refinement of $n_x = 512$ and $\Delta t = 10^{-6}$ s, still yielding a CFL number $\sigma \approx 0.65$. The system is now evolved for 10^{-4} s. We compute the L_1 -norm of the difference between two consecutive iterates for the key variables as a function of the number of sweeps. The result, shown in Fig. 10, is consistent with those of Sections 4 and 5.2. The MISDC sweeps fail to converge to a fixed point solution because of the stiffness of the DME chemistry mechanism. This is particularly visible after sweep 15 in Figs. 10(c) and 10(d). The other schemes achieve convergence at different rates. CISDCQ-3 and CISDCQ-4 have practically converged at sweep 20. But, for CISDCQ-2 and MISDCQ, the convergence rate is relatively slower and more than 40 sweeps are required to reach convergence (not shown in Fig. 10).

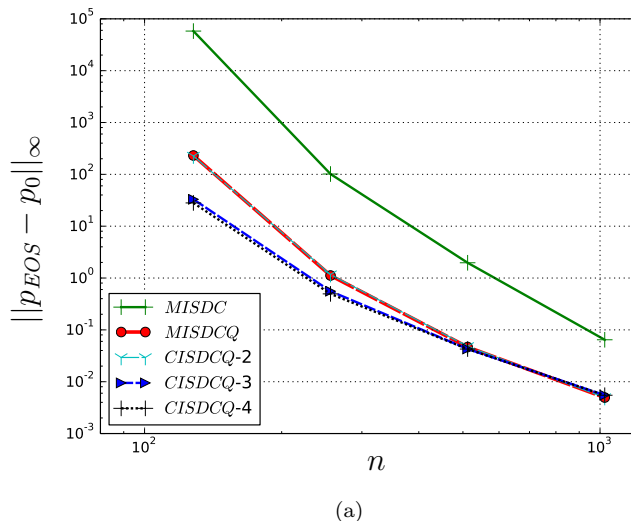


Figure 9: Convergence of the L_∞ -norm of the thermodynamic drift as a function of the level of space-time refinement at the end of the DME flame simulation.

Using the same methodology as in Section 5.2, we compare the respective computational costs of the schemes after 20 and after 25 sweeps for the density (Fig. 10). The computational cost ratios R_ν are in Table 5. We find that the convergence of the sweeps to a fixed-point solution is too slow to achieve a computational cost reduction when only two nested iterations are used ($R_{\nu=2} = 0.8$ after 25 sweeps). But, with three iterations, the significantly faster convergence of the sweeps leads to a reduction in computational cost ($R_{\nu=3} = 1.6$ after 25 sweeps). Finally, using four nested iterations does not improve the ratio R_ν due to the increase in the cost of the sweep ($S_{\nu=4} = 1.2$ after 25 sweeps). As stated before, an adaptive method to vary the number of nested iterations on ℓ at each sweep would increase, up to a certain extent, the computational cost reduction obtained with CISDCQ.

N_M	$R_{\nu=2}$	$R_{\nu=3}$	$R_{\nu=4}$
20 sweeps	0.8	1.4	1.1
25 sweeps	0.8	1.6	1.2

Table 5: Ratio of the computational cost of MISDCQ over that of CISDCQ- ν for the DME flame simulation after 20 sweeps and after 25 sweeps.

6. Conclusions

In this work, we consider the time integration of the advection-diffusion-reaction systems arising from the spatial discretization of the equations governing low-Mach number combustion with complex chemistry. The problem is advanced in time on the scale of the relatively slow advection process, which makes it challenging to efficiently capture the nonlinear coupling with the faster diffusion and reaction processes. In the serial MISDC algorithm of Pazner et al. (2016), this entails solving expensive implicit diffusion and reaction systems at each substep. We first present an improved multi-implicit scheme, MISDCQ, whose sweeps retain excellent convergence properties on stiff problems. Then, to reduce the time-to-solution, we modify MISDCQ to design a parallel-across-the-method integration scheme based on spectral deferred corrections. The scheme, referred to as Concurrent Implicit SDCQ (CISDCQ), is obtained by decoupling the diffusion step from the reaction step in serial MISDCQ. This allows concurrent implicit diffusion and reaction solves performed by different processors to reduce the time-to-solution.

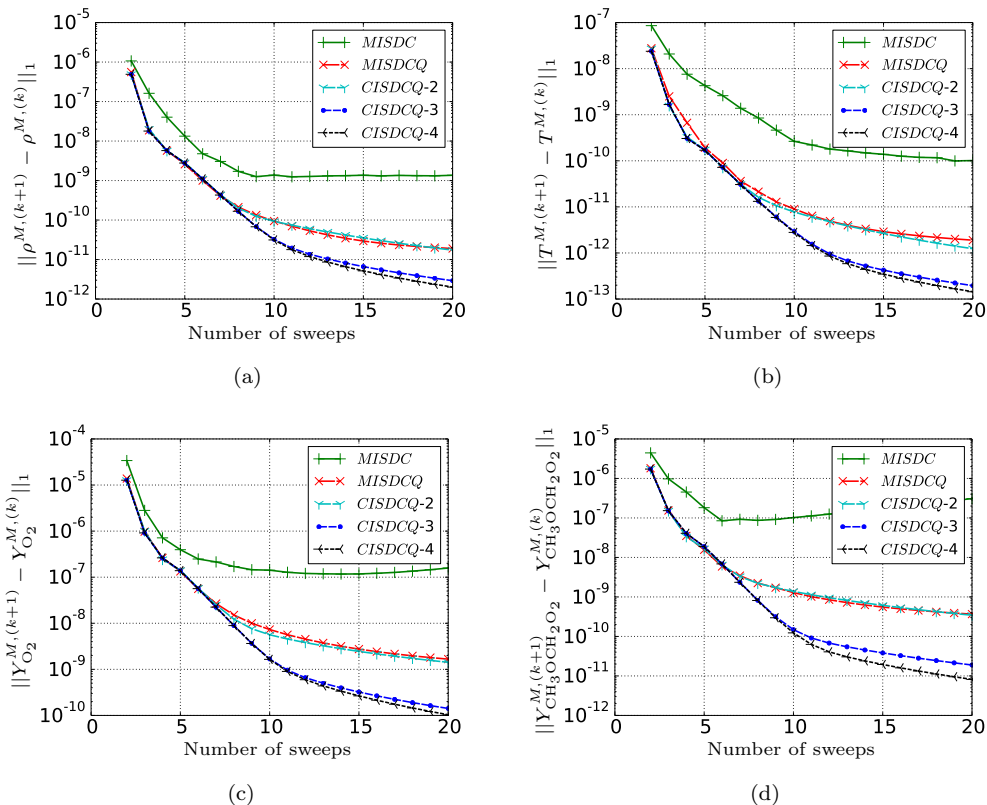


Figure 10: Convergence of the L_1 -norm of the difference between two consecutive iterates for the last time step of the DME flame simulation performed with $n_x = 512$ control volumes. The density, temperature, and mass fractions Y_{O_2} and $Y_{CH_3OCH_2O_2}$ are in Figs. 10(a), 10(b), 10(c), and 10(d), respectively.

We study the accuracy, stability, convergence rate, and theoretical computational cost of the proposed parallel scheme. The linear convergence analysis demonstrates that CISDCQ is stable for stiff problems and that the CISDCQ iterative correction process can converge at a faster rate than that of the standard serial MISDC scheme. We propose a numerical methodology to apply CISDCQ to the discretized low-Mach number equation set with complex chemistry. The numerical results – including a stiff premixed flame simulation – confirm the findings of the convergence analysis and demonstrate the robustness and parallel efficiency of the new scheme.

Future work includes extending the method presented here to multidimensional simulations. In multiple dimensions, the efficiency of the scheme could be improved by exploiting local variations in temporal stiffness. We plan to exploit local variabilities by combining SDC-based algorithms (CISDC, and Multi-Level SDC of Speck et al. (2015)) with block-structured adaptive refinement techniques, which will be used to concentrate the computational effort – small time steps and finer spatial meshing – near local structures in the flow. This will allow us to simultaneously deal with variability in temporal and spatial resolution requirements, which typically are coincident in combustion problems. A further improvement would consist in amortizing the cost of the fine sweeps by performing them in parallel, as in the Parallel Full Approximation Scheme in Space and in Time (PFASST) scheme (Emmett and Minion, 2012).

As a final note, we mention an important but somewhat indirect benefit of our proposed concurrent update scheme. Linear solvers play a key role in the implementation of the low-Mach projection algorithm in multiple dimensions, both for the implicit diffusion and for the velocity projection operators. However, linear solvers are notoriously difficult to scale up to the large processor counts typical of modern massively parallel computing hardware. But because each of the algorithmic components in our scheme are managed by a partitioned subset of the processors working in an “embarrassingly parallel” mode with the other partitions, the requirements of the combined algorithm are reduced directly, by a factor equal to the number of available concurrent tasks. In the DME model discussed in this work for example,

the implicit diffusion of 39 chemical species can be performed independently, *and* independent of the chemistry integration. While the parallelization of the diffusion step over the species can be implemented in the original MISDC scheme, the results in this paper verify that we have developed an algorithm that will allow unique access to a new axis of parallelism. Whether it can be exploited effectively depends on the cost of communicating the subproblems across the machine, relative to the gains afforded by the smaller pool of compute processors. Exploration of that trade-off will be the subject of future work.

Funding

This research was supported by the Applied Mathematics Program of the U.S. DOE Office of Advanced Scientific Computing Research under contract number DE-AC02-05CH11231. Some computations used the resources of the National Energy Research Scientific Computing Center, a DOE Office of Science User Facility supported by the Office of Science of the U.S. DOE under Contract No. DE-AC02-05CH11231.

Appendix A. Derivation of the CISDCQ iteration matrix

We prove by induction on ℓ and m that the matrix form of the CISDCQ update equations (26)-(27) leads to a relationship between $\Phi_{m+1}^{(k+1,\ell+1)}$ and $\Phi^{(k)}$ in the form of (58). We first introduce the matrices

$$\mathbf{A}_{\kappa,m+1} := \mathbf{I} - \kappa \Delta t \mathbf{D}_{m+1} \tilde{\mathbf{Q}}^I, \quad \kappa = \{d, r\} \quad (\text{A.1})$$

where $\mathbf{I} \in \mathbb{R}^{M \times M}$ is the identity matrix, and $\mathbf{D}_{m+1} \in \mathbb{R}^{M \times M}$ contains only one non-zero entry, equal to one, in slot $(m+1, m+1)$, with the convention that $\mathbf{D}_0 = \mathbf{0}$. We first consider the first nested iteration ($\ell = 0$). With the initialization procedure of (28) to (30), the diffusion update (26) in matrix form reads

$$\begin{aligned} \mathbf{D}_{m+1} \Phi_{AD,m+1}^{(k+1,1)} &= \mathbf{D}_{m+1} [\phi^0 \mathbf{1} + s \Delta t \phi^0 \mathbf{q} + \Delta t (s \tilde{\mathbf{Q}} - a \tilde{\mathbf{Q}}^E - (d+r) \tilde{\mathbf{Q}}^I) \Phi^{(k)}] \\ &\quad + a \Delta t \mathbf{D}_{m+1} \tilde{\mathbf{Q}}^E ((\mathbf{I} - \mathbf{D}_m) \Phi_m^{(k+1,1)} + \mathbf{D}_m \Phi_{AD,m+1}^{(k+1,1)}) \\ &\quad + d \Delta t \mathbf{D}_{m+1} \tilde{\mathbf{Q}}^I ((\mathbf{I} - \mathbf{D}_m) \Phi_m^{(k+1,1)} + \mathbf{D}_m \Phi_{AD,m+1}^{(k+1,1)} + \mathbf{D}_{m+1} \Phi_{AD,m+1}^{(k+1,1)}) \\ &\quad + r \Delta t \mathbf{D}_{m+1} \tilde{\mathbf{Q}}^I ((\mathbf{I} - \mathbf{D}_m) \Phi_m^{(k+1,1)} + (\mathbf{D}_m + \mathbf{D}_{m+1}) \Phi_{m+1}^{(k+1,0)}). \end{aligned} \quad (\text{A.2})$$

By construction of the vectors $\Phi_{m+1}^{(k+1,\ell+1)}$ and $\Phi_{AD,m+1}^{(k+1,\ell+1)}$, only the $(m+1)^{\text{th}}$ entry is modified at the $(m+1)^{\text{th}}$ substep. Therefore, the following equalities hold

$$(\mathbf{I} - \mathbf{D}_{m+1}) \Phi_{AD,m+1}^{(k+1,\ell+1)} = \Phi_{AD,m}^{(k+1,\ell+1)}, \quad (\text{A.3})$$

$$(\mathbf{I} - \mathbf{D}_{m+1}) \Phi_{m+1}^{(k+1,\ell+1)} = \Phi_m^{(k+1,\ell+1)}. \quad (\text{A.4})$$

Summing (A.2) and (A.3), and then multiplying the resulting equation by $\mathbf{A}_{d,m+1}^{-1}$, we obtain

$$\begin{aligned} \Phi_{AD,m+1}^{(k+1,1)} &= \mathbf{A}_{d,m+1}^{-1} \mathbf{D}_{m+1} [\phi^0 \mathbf{1} + s \Delta t \phi^0 \mathbf{q} + \Delta t (s \tilde{\mathbf{Q}} - a \tilde{\mathbf{Q}}^E - (d+r) \tilde{\mathbf{Q}}^I) \Phi^{(k)}] \\ &\quad + \mathbf{A}_{d,m+1}^{-1} (\mathbf{B}_{m+1} \Phi_m^{(k+1,1)} + \mathbf{C}_{m+1} \Phi_{AD,m}^{(k+1,1)} + \mathbf{E}_{m+1} \Phi_{m+1}^{(k+1,0)}), \end{aligned} \quad (\text{A.5})$$

where the matrices \mathbf{B}_{m+1} , \mathbf{C}_{m+1} , and \mathbf{E}_{m+1} depend on the matrices $\tilde{\mathbf{Q}}$, $\tilde{\mathbf{Q}}^I$, and $\tilde{\mathbf{Q}}^E$, and on the scalars m , Δt , a , d , and r . The expression of these matrices is omitted for brevity. Next, we consider the reaction update. In matrix form, the reaction update (27) is

$$\mathbf{D}_{m+1} \Phi_{m+1}^{(k+1,1)} = \mathbf{D}_{m+1} \Phi_{AD,m+1}^{(k+1,1)} + r \Delta t \mathbf{D}_{m+1} \tilde{\mathbf{Q}}^I (\mathbf{D}_m + \mathbf{D}_{m+1}) (\Phi_{m+1}^{(k+1,1)} - \Phi_{m+1}^{(k+1,0)}), \quad (\text{A.6})$$

which gives, after using (A.5) to eliminate $\Phi_{AD,m+1}^{(k+1,1)}$,

$$\begin{aligned} \mathbf{D}_{m+1} \Phi_{m+1}^{(k+1,1)} &= \mathbf{D}_{m+1} \mathbf{A}_{d,m+1}^{-1} \mathbf{D}_{m+1} [\phi^0 \mathbf{1} + s \Delta t \phi^0 \mathbf{q} + \Delta t (s \tilde{\mathbf{Q}} - a \tilde{\mathbf{Q}}^E - (d+r) \tilde{\mathbf{Q}}^I) \Phi^{(k)}] \\ &\quad + \mathbf{D}_{m+1} \mathbf{A}_{d,m+1}^{-1} (\mathbf{B}_{m+1} \Phi_m^{(k+1,1)} + \mathbf{C}_{m+1} \Phi_{AD,m}^{(k+1,1)} + \mathbf{E}_{m+1} \Phi_m^{(k+1,0)}) \\ &\quad + r \Delta t \mathbf{D}_{m+1} \tilde{\mathbf{Q}}^I (\mathbf{D}_m + \mathbf{D}_{m+1}) (\Phi_{m+1}^{(k+1,1)} - \Phi_{m+1}^{(k+1,0)}). \end{aligned} \quad (\text{A.7})$$

Summing (A.4) and (A.7), and then multiplying the equation by $\mathbf{A}_{r,m+1}^{-1}$ leads to

$$\begin{aligned} \Phi_{m+1}^{(k+1,1)} &= \mathbf{A}_{r,m+1}^{-1} \mathbf{D}_{m+1} \mathbf{A}_{d,m+1}^{-1} \mathbf{D}_{m+1} [\phi^0 \mathbf{1} + s \Delta t \phi^0 \mathbf{q} + \Delta t (s \tilde{\mathbf{Q}} - a \tilde{\mathbf{Q}}^E - (d+r) \tilde{\mathbf{Q}}^I) \Phi^{(k)}] \\ &\quad + \mathbf{A}_{r,m+1}^{-1} (\mathbf{R}_{m+1} \Phi_m^{(k+1,1)} + \mathbf{S}_{m+1} \Phi_{AD,m}^{(k+1,1)} + \mathbf{T}_{m+1} \Phi_{m+1}^{(k+1,0)}). \end{aligned} \quad (\text{A.8})$$

The expressions of \mathbf{R}_{m+1} , \mathbf{S}_{m+1} , and \mathbf{T}_{m+1} are obtained using (A.7). They depend on the matrices $\tilde{\mathbf{Q}}$, $\tilde{\mathbf{Q}}^I$, and $\tilde{\mathbf{Q}}^E$, and on m , Δt , a , d , and r . Considering that $(\mathbf{D}_m + \mathbf{D}_{m+1}) \Phi_{m+1}^{(k+1,0)} = (\mathbf{D}_m + \mathbf{D}_{m+1}) \Phi^{(k)}$, we can use (A.5)-(A.8) to show by induction on m that (58) holds for $\ell = 0$ and derive the expressions for $\mathbf{M}_{1,m+1}^{(1)}$, $\mathbf{M}_{2,m+1}^{(1)}$, $\mathbf{N}_{1,m+1}^{(1)}$, and $\mathbf{N}_{2,m+1}^{(1)}$. The proof for $\ell \geq 1$ is analogous and is omitted here.

References

- Bansal, G., Mascarenhas, A., and Chen, J. H. (2015). Direct numerical simulations of autoignition in stratified dimethyl-ether (DME)/air turbulent mixtures. *Combustion and Flame*, 162(3):688–702.
- Bourlioux, A., Layton, A. T., and Minion, M. L. (2003). High-order multi-implicit spectral deferred correction methods for problems of reactive flow. *Journal of Computational Physics*, 189(2):651–675.
- Burrage, K. (1997). Parallel methods for ODEs. *Advances in Computational Mathematics*, 7(1-2):1–31.
- Butcher, J. C. (1997). Order and stability of parallel methods for stiff problems. *Advances in Computational Mathematics*, 7(1):79–96.
- Christlieb, A. J., Haynes, R. D., and Ong, B. W. (2012). A parallel space-time algorithm. *SIAM Journal on Scientific Computing*, 34(5):C233–C248.
- Christlieb, A. J., Macdonald, C. B., and Ong, B. W. (2010). Parallel high-order integrators. *SIAM Journal on Scientific Computing*, 32(2):818–835.
- Christlieb, A. J., Ong, B. W., and Qiu, J.-M. (2009). Comments on high-order integrators embedded within integral deferred correction methods. *Communications in Applied Mathematics and Computational Science*, 4(1):27–56.
- Day, M. S. and Bell, J. B. (2000). Numerical simulation of laminar reacting flows with complex chemistry. *Combustion Theory and Modelling*, 4(4):535–556.
- Duarte, M., Descombes, S., Tenaud, C., Candel, S., and Massot, M. (2013). Time-space adaptive numerical methods for the simulation of combustion fronts. *Combustion and Flame*, 160(6):1083–1101.
- Dutt, A., Greengard, L., and Rokhlin, V. (2000). Spectral deferred correction methods for ordinary differential equations. *BIT Numerical Mathematics*, 40(2):241–266.
- Emmett, M. and Minion, M. L. (2012). Toward an efficient parallel in time method for partial differential equations. *Communications in Applied Mathematics and Computational Science*, 7(1):105–132.
- Falgout, R. D., Friedhoff, S., Kolev, T. V., MacLachlan, S. P., and Schroder, J. B. (2014). Parallel time integration with multigrid. *SIAM Journal on Scientific Computing*, 36(6):C635–C661.
- Gander, M. J. (1999). A waveform relaxation algorithm with overlapping splitting for reaction diffusion equations. *Numerical Linear Algebra with Applications*, 6(2):125–145.
- Hagstrom, T. and Zhou, R. (2007). On the spectral deferred correction of splitting methods for initial value problems. *Communications in Applied Mathematics and Computational Science*, 1(1):169–205.
- Iserles, A. and Nørsett, S. P. (1990). On the theory of parallel Runge-Kutta methods. *IMA Journal of Numerical Analysis*, 10(4):463–488.
- Kee, R. J., Grcar, J. F., Smooke, M. D., Miller, J. A., and Meeks, E. (1985). PREMIX: a Fortran program for modeling steady laminar one-dimensional premixed flames. Technical report, Sandia National Laboratory, USA.
- Kee, R. J., Warnatz, J., and Miller, J. A. (1983). Fortran computer-code package for the evaluation of gas-phase viscosities, conductivities, and diffusion coefficients. Technical report, Sandia National Laboratory, USA.
- Knio, O. M., Najm, H. N., and Wyckoff, P. S. (1999). A semi-implicit numerical scheme for reacting flow: Ii. stiff, operator-split formulation. *Journal of Computational Physics*, 154(2):428–467.
- Layton, A. T. and Minion, M. L. (2004). Conservative multi-implicit spectral deferred correction methods for reacting gas dynamics. *Journal of Computational Physics*, 194(2):697–715.

- Lelarasme, E., Ruehli, A. E., and Sangiovanni-Vincentelli, A. L. (1982). The waveform relaxation method for time-domain analysis of large scale integrated circuits. *IEEE Transactions on Computer-Aided Design of Integrated Circuits and Systems*, 1(3):131–145.
- Lions, J.-L., Maday, Y., and Turinici, G. (2001). Résolution d’EDP par un schéma en temps pararéel. *Comptes Rendus de l’Académie des Sciences-Series I-Mathematics*, 332(7):661–668.
- Majda, A. and Sethian, J. (1985). The derivation and numerical solution of the equations for zero Mach number combustion. *Combustion Science and Technology*, 42(3-4):185–205.
- McCorquodale, P. and Colella, P. (2011). A high-order finite-volume method for conservation laws on locally refined grids. *Communications in Applied Mathematics and Computational Science*, 6(1):1–25.
- Minion, M. L. (2003). Semi-implicit spectral deferred correction methods for ordinary differential equations. *Communications in Mathematical Sciences*, 1(3):471–500.
- Miranker, W. L. and Liniger, W. (1967). Parallel methods for the numerical integration of ordinary differential equations. *Mathematics of Computation*, 21(99):303–320.
- Motheau, E. and Abraham, J. (2016). A high-order numerical algorithm for DNS of low-mach-number reactive flows with detailed chemistry and quasi-spectral accuracy. *Journal of Computational Physics*, 313:430–454.
- Najm, H. N. and Knio, O. M. (2005). Modeling low mach number reacting flow with detailed chemistry and transport. *Journal of Scientific Computing*, 25(1-2):263.
- Najm, H. N., Wyckoff, P. S., and Knio, O. M. (1998). A semi-implicit numerical scheme for reacting flow: I. stiff chemistry. *Journal of Computational Physics*, 143(2):381–402.
- Nievergelt, J. (1964). Parallel methods for integrating ordinary differential equations. *Communications of the ACM*, 7(12):731–733.
- Nonaka, A., Bell, J. B., Day, M. S., Gilet, C., Almgren, A. S., and Minion, M. L. (2012). A deferred correction coupling strategy for low Mach number flow with complex chemistry. *Combustion Theory and Modelling*, 16(6):1053–1088.
- Pazner, W. E., Nonaka, A., Bell, J. B., Day, M. S., and Minion, M. L. (2016). A high-order spectral deferred correction strategy for low Mach number flow with complex chemistry. *Combustion Theory and Modelling*, 20(3):521–547.
- Pember, R. B., Howell, L. H., Bell, J. B., Colella, P., Crutchfield, W. Y., Fiveland, W. A., and Jessee, J. P. (1998). An adaptive projection method for unsteady, low-mach number combustion. *Combustion Science and Technology*, 140(1-6):123–168.
- Perini, F., Galligani, E., and Reitz, R. D. (2012). An analytical Jacobian approach to sparse reaction kinetics for computationally efficient combustion modeling with large reaction mechanisms. *Energy & Fuels*, 26(8):4804–4822.
- Rehm, R. G. and Baum, H. R. (1978). The equations of motion for thermally driven buoyant flows. *Journal of Research of the National Bureau of Standards*, 83:297–308.
- Safta, C., Ray, J., and Najm, H. N. (2010). A high-order low-mach number AMR construction for chemically reacting flows. *Journal of Computational Physics*, 229(24):9299–9322.
- Speck, R. (2017). Parallelizing spectral deferred corrections across the method. *arXiv preprint arXiv:1703.08079*.
- Speck, R., Ruprecht, D., Emmett, M., Minion, M. L., Bolten, M., and Krause, R. (2015). A multi-level spectral deferred correction method. *BIT Numerical Mathematics*, 55(3):843–867.
- Warnatz, J. and Peters, N. (1982). Numerical methods in laminar flame propagation. *Vieweg, Braunschweig*, pages 87–111.
- Weiser, M. (2015). Faster SDC convergence on non-equidistant grids by DIRK sweeps. *BIT Numerical Mathematics*, 55(4):1219–1241.
- Xia, Y., Xu, Y., and Shu, C. (2007). Efficient time discretization for local discontinuous Galerkin methods. *Discrete and Continuous Dynamical Systems Series B*, 8(3):677.
- Zhang, Q., Johansen, H., and Colella, P. (2012). A fourth-order accurate finite-volume method with structured adaptive mesh refinement for solving the advection-diffusion equation. *SIAM Journal on Scientific Computing*, 34(2):B179–B201.